Water Air Soil Pollut (2026) 237:377
https://doi.org/10.1007/s11270-025-09054-z

Machine Learning-Guided Prediction and Interpretation of Rhodamine B Removal by Biochar Derived from Marine Biomass

Dilek Gümüş · Fatih Gümüş · Elif Nihan Kadioğlu · Handan Atalay Eroğlu

Received: 11 July 2025 / Accepted: 20 December 2025 / Published online: 10 January 2026
© The Author(s), under exclusive licence to Springer Nature Switzerland AG 2026

Abstract This study aims to provide a sustainable solution for dye removal by developing environmentally friendly and renewable resource-based adsorbents. In this context, the removal of Rhodamin B (RhB) dye from aqueous solutions was investigated using composite biochar obtained from the seaweed species *Ulva lactuca –Cystoseira* sensu lato. The characterization of the adsorbent, which draws attention with its high surface area (797.91 m^2/g), porous structure and rich functional groups, was carried out by SEM, FTIR and BET analyses. The data obtained as a result of adsorption experiments were evaluated with kinetic and isotherm models; the pseudo-second-order kinetic model ($R^2 = 0.993$) and Freundlich isotherm ($R^2 = 0.994$) successfully reflected the chemical and multi-layered nature of the process. In this context, the adsorption data were modelled with four different machine learning algorithms (Random Forest, XGBoost, CatBoost, Gradient Boosting). Among the models, Random Forest algorithm showed the highest accuracy on the test data ($R^2 = 0.93$, RMSE = 4.15, MAE = 1.95) and successfully reflected the behaviour of the system. The decision mechanisms of the model were explained with SHAP analysis; the dominant effects of contact time and adsorption capacity on the prediction were determined. While PDP analyses visualized the individual effects of variables on the target variable, learning curves and residual analyses confirmed the generalization ability and stability of the Random Forest model. This multi-faceted approach shows that both biomass wastes can be converted into environmentally friendly adsorbents and machine learning-based methods can be used effectively in water treatment applications.

Keywords Adsorption · Rhodamine B · Composite biochar · Machine Learning · SHAP analysis

D. Gümüş (✉)
Environmental Engineering Department, Faculty of Engineering And Architecture, Sinop University, 57000 Sinop, Türkiye
e-mail: dgumus@sinop.edu.tr

F. Gümüş
Department of Biology, Faculty of Arts and Science, Sinop University, 57000 Sinop, Türkiye

E. N. Kadioğlu
Environmental Engineering Department, Ondokuz Mayıs University, Engineering Faculty, 55139, Kurupelit, Samsun, Türkiye

H. A. Eroğlu
Environmental Engineering Department, Ondokuz Mayıs University, Engineering Faculty, 55139, Kurupelit, Samsun, Türkiye

1 Introduction

The contamination of water bodies with synthetic dyes has become one of the most persistent environmental problems of the modern industrial era. As

global industries such as textiles, cosmetics, plastics, and food processing continue to expand, large volumes of wastewater containing non-biodegradable colorants are discharged into natural aquatic systems without adequate treatment. These compounds are not only aesthetically undesirable, but they also interfere with photosynthetic activity in aquatic ecosystems, reduce sunlight penetration, and pose potential toxic effects to aquatic life and humans (Crini & Lichtfouse, 2019; Kayranli, 2025). Rhodamine B (RhB) is a prime example of such dyes. It is widely used due to its strong fluorescence, thermal stability, and cost-effectiveness. However, RhB is known to exhibit carcinogenic, teratogenic, and mutagenic effects. Once it enters aquatic systems, it tends to persist due to its resistance to natural degradation processes. Even at low concentrations, RhB can cause oxidative stress and DNA damage in aquatic organisms, raising serious ecological and health concerns (Kapoor et al., 2024; Lin et al., 2020). Consequently, its efficient and safe removal from water streams remains a major focus in environmental protection.

Various physical, chemical, and biological methods have been developed to remove RhB and similar compounds from water. However, each technique has specific limitations. Biological treatments are often inefficient for synthetic dyes because of their complex aromatic structures and low biodegradability. Advanced oxidation processes (AOPs) and membrane-based technologies offer higher efficiencies but are often energy-intensive, costly, or require advanced infrastructure. Moreover, these processes can sometimes generate hazardous by-products that require further treatment before discharge (Mayilswamy et al., 2025; Mohan et al., 2014; Tan et al., 2015). In contrast, adsorption has emerged as a simple, effective, and scalable method for dye removal from aqueous media. It allows for easy operation, minimal sludge generation, and the possibility of reusing or regenerating the adsorbent. The success of the adsorption process is strongly dependent on the characteristics of the adsorbent material (Ashraf et al., 2024; Tan et al., 2015).

Over the past decade, biochar has gained increasing attention as a low-cost, carbon-rich, and porous material produced by pyrolysis of biomass under oxygen-limited conditions. Its large surface area, chemical stability, and abundant surface functional groups make it suitable for pollutant adsorption, including dyes (Ahmad et al., 2014; Behera et al., 2024). Traditionally, biochar has been synthesized from lignocellulosic biomass such as sawdust, rice husks, and agricultural waste. However, recent studies have explored non-traditional biomass sources, particularly marine macro algae such as *U. lactuca* and *Cystoseira s.l.*, due to their rapid growth, high mineral content, and underutilization (Inyang et al., 2016; Ravindiran et al., 2024).

In addition to raw biochar, composite biochar, which are biochar enhanced with inorganic or organic materials, have shown significantly improved adsorption performance. These composites often involve the incorporation of metal oxides (e.g., Fe_3O_4, ZnO), clays, or polymers during synthesis, resulting in enhanced surface reactivity, pore structure, and affinity for specific pollutants (Yadav et al., 2025; Zhao et al., 2022). Composite biochar derived from marine algae combines the inherent adsorption properties of seaweed-based carbon with the enhanced functionalities offered by the modifying agents, leading to superior dye removal capacity. The high ash content and natural presence of elements such as Ca, Mg, and Fe in macro algae further contribute to ion exchange and electrostatic interactions with dye molecules. Such composite structures not only offer improved performance but also align with the goals of sustainable water treatment and circular bio economy by converting underutilized marine biomass into high-value environmental materials (Foong et al., 2023; Niedzbała et al., 2024). Furthermore, utilizing seaweed as a biomass source mitigates the competition with land-based food crops, addressing one of the major sustainability challenges associated with conventional biochar production. Marine macro algae such as *U. lactuca* and *Cystoseira s.l.* grow rapidly, require no arable land or freshwater, and are often regarded as underutilized resources, making them ideal candidates for sustainable biochar development. However, despite the promising characteristics of composite biochar derived from such feedstock's, their adsorption performance is governed by a multitude of interdependent factors—including solution pH, initial dye concentration, contact time, temperature, and adsorbent dosage. These variables often interact in highly nonlinear and system-specific ways, which limits the capacity of classical kinetic and isotherm models—such as Langmuir, Freundlich, or pseudo-first-order equations—to fully capture the

dynamic adsorption behaviour. These traditional models generally rely on fixed assumptions and simplified mathematical relationships that may not accurately reflect the complexity of real-world adsorption systems (Soares Dias et al., 2025).

To overcome these limitations, researchers have increasingly adopted machine learning (ML) techniques, which can capture complex, nonlinear relationships within multidimensional datasets (Zhang et al., 2023; Zhao et al., 2022). ML algorithms such as Random Forest (RF), Gradient Boosting (GB) and Support Vector Regression (SVR) provide not only high prediction accuracy but also insights into variable importance and interaction effects—offering both predictive and interpretive power.

The present study aims to bridge the existing research gap by investigating the adsorption behaviour of Rhodamine B onto composite biochar synthesized from the marine macro algae species *U. lactuca* and *Cystoseira s.l.*. Specifically, the objectives of this research are to: (i) synthesize and comprehensively characterize marine macro algae-based composite biochar, (ii) evaluate their dye removal performance under a range of experimental conditions, and (iii) develop, compare, and interpret the predictive capabilities of machine learning models, including Random Forest (RF), Gradient Boosting (GBM), XGBoost, and CatBoost. Particular emphasis is placed not only on predictive accuracy but also on model interpretability through SHAP and PDP analyses, enabling detailed insights into the relative importance and marginal effects of individual features. By integrating sustainable adsorbent development with explainable, data-driven modelling approaches, this study offers a robust framework for the design of intelligent and eco-friendly solutions for dye-contaminated wastewater treatment.

2 Materials and Method

2.1 Materials

Biomass samples of *U. lactuca* and *Cystoseira s.l.* were collected from the coastal waters of Sinop Province, situated along the Black Sea region of Türkiye. Analytical grade reagents were utilized throughout the experiments, all of which were procured from Merck (Germany). These included sodium hydroxide (NaOH, ≥ 97%), phosphoric acid (H_3PO_4, 85% w/w), potassium nitrate (KNO_3, ≥ 97%), and hydrochloric acid (HCl, 37% w/w). Deionized water was used in all experimental steps to prevent any contamination or interference from impurities.

Rhodamine B ($C_{28}H_{31}ClN_2O_3$; molecular weight: 479.01 g/mol; λ_{max}: 554 nm) was employed as the model organic contaminant to evaluate the adsorption characteristics of the synthesized composite biochar. A stock solution of Rhodamine B (1.0 g/L) was prepared by dissolving an accurately weighed amount of dye in deionized water, followed by storage in a dark environment at ambient temperature. Working solutions with varying initial concentrations were prepared by serial dilution of the stock solution immediately prior to use.

2.2 Preparation of Composite Biochar Adsorbent

The activated biochar was synthesized using a single-step microwave-assisted method, adapted with minor modifications from a previously reported procedure (Gümüş & Gümüş, 2022). A novel composite biochar (hereafter referred to as UCAC) was synthesized from a 1:1 (w/w) blend of *U. lactuca* and *Cystoseira s.l.*, two widely available macroalgal species. Freshly collected biomass samples were thoroughly rinsed with ultrapure water to eliminate surface impurities such as sand, salt, and organic debris. After cleaning, the biomass was oven-dried at 105 °C for 24 h using a laboratory oven (Nüve FN 300) to ensure moisture removal. The dried material was then ground into powder using an electric grinder (Waring 8011). The powdered algal mixture was impregnated with H_3PO_4 at a mass-to-volume ratio of 1:10 (g/mL). The prepared slurry was continuously stirred at room temperature for a duration of 24 h at 150 rpm to promote chemical activation. After the impregnation period, the mixture was transferred into a quartz-glass reactor and subjected to pyrolysis in a household microwave oven (700 W) for a total of 18 min, divided into three cycles of 6 min each, under oxygen-limited conditions to prevent combustion. The pyrolyzed product was then allowed to cool at room temperature, completing the one-step microwave-assisted activation process.

2.3 Characterization of UCAC

Surface functional groups of UCAC before and after dye adsorption were identified using Fourier Transform Infrared Spectroscopy (FTIR) (Shimadzu, IRSpirit) in the scanning range of 400–4000 cm^{-1}. Morphological features were visualized through Scanning Electron Microscopy (SEM) (Zeiss Sigma 300), which provided detailed images of the surface texture and porosity. The specific surface area and pore properties were quantified via Brunauer–Emmett–Teller (BET) analysis (Quantachrome Nova Touch LX4). Prior to nitrogen adsorption, samples were degassed at 300 °C under vacuum for 6 h to eliminate any adsorbed moisture or impurities.

The point of zero charge (pH_pzc) of the UCAC adsorbent was determined following the procedure adapted from Hoang et al. (2024). In brief, a series of 0.1 M KNO_3 solutions (30 mL each) were prepared, and their initial pH values (pH_i) were adjusted between 3.0 and 10.0 using either 0.1 M HCl or 0.1 M NaOH. Subsequently, 0.05 g of UCAC was introduced into each solution, and the mixtures were stirred continuously for 24 h at room temperature to reach equilibrium. After equilibration, the final pH (pH_f) values were measured. The pH_{pzc} of UCAC was identified from the plot of ΔpH ($pH_i - pH_f$) versus the initial pH, where the curve intersected the line $\Delta pH = 0$.

2.4 Batch Adsorption Studies

Batch-mode adsorption experiments were conducted to evaluate the removal efficiency of Rhodamine B by UCAC under varying operational parameters. All experimental procedures were conducted using 100 mL Erlenmeyer flasks, with each flask containing 50 mL of the dye solution, and the mixtures were agitated on an orbital shaker at 150 rpm at a room temperature of 24 ± 1 °C. The effects of initial solution pH, initial dye concentration, adsorbent dosage, and contact time were examined. The pH of the solutions was adjusted in the range of 3 to 8 using 0.1 M HCl or 0.1 M NaOH. Adsorbent dosages were varied between 0.05 and 1.5 g/L, while initial Rhodamine B concentrations of 20 mg/L. Contact time were studied in the range of 0 to 150 min to determine the kinetic behaviour. Kinetic experiments were performed at a fixed adsorbent dose of 0.2 g/L and solution pH of 6, using two initial dye concentrations: 10 mg/L and 20 mg/L. Samples were collected at predetermined time intervals and filtered immediately to separate the adsorbent. For isotherm studies, the initial dye concentration was varied from 10 to 50 mg/L, while the adsorbent dosage (0.2 g/L), solution pH (6), and contact time (90 min) were kept constant. The concentration of Rhodamine B remaining in solution was determined spectrophotometrically at $\lambda_{max} = 554$ nm using a UV–Vis spectrophotometer (Thermo Genesys 10). All experiments were conducted in duplicate, and average values were reported.

The adsorption capacity (q_e) and removal efficiency (% Removal) were calculated according to the following equations:

$$q_e = \frac{C_0 - C_e}{m} * V \quad (1)$$

$$\%\ \text{Removal} = \frac{C_0 - C_e}{C_0} * 100 \quad (2)$$

The equilibrium data obtained from the isotherm experiments were fitted to Langmuir and Freundlich isotherm models to describe the adsorption behaviour of Rhodamine B onto the UCAC surface. The experimental kinetic data were fitted to the pseudo-first-order (PFO) and pseudo-second-order (PSO) equations to assess adsorption behaviour.

After adsorption experiments performed under optimal conditions, spent UCAC was recovered by centrifugation and used in regeneration experiments. It was treated with methanol three times to desorb retained dye molecules. After desorption, the adsorbent was rinsed thoroughly with deionized water and oven-dried at 50 °C for 12 h. The regenerated adsorbent was reused in up to five consecutive adsorption–desorption cycles to evaluate its reusability performance.

2.5 Machine Learning Model Development

2.5.1 Dataset and Variable Definitions

The dataset used in this study consists of 110 observations obtained as a result of laboratory-scale adsorption experiments and representing the removal performance of Rhodamine B (RhB) dye under different conditions. Each record contains the removal

efficiency (removal efficiency, %) of the system under certain operational conditions and the input parameters corresponding to these conditions. In the model, the pH representing the acidic/basic character of the solution, the biochar dose defining the amount of applied biochar (g/L), the initial dye concentration (mg/L), the contact time during which adsorption occurs (min) and the adsorption capacity showing how much dye the adsorbent can adsorb per unit mass (mg/g) were used as independent variables. The "Removal Efficiency (%)" representing the total removal performance of the system was selected as the dependent variable (target variable).

A random shuffling procedure was applied to homogenize variable distributions before splitting, and a fixed random seed (42) was used in all modelling stages to ensure reproducibility. Although the dataset size (110) remains moderate, it is comparable to or larger than sample sizes commonly reported in recent ML-based adsorption research, supporting reliable model training. To further minimize variance arising from random partitioning and to ensure robust generalization, five-fold and repeated ten-fold cross-validation schemes were employed throughout the modelling process.

2.5.2 *Data Pre-Processing*

Data analysis and modelling steps were performed in Python 3.10 environment using Jupyter Notebook platform. First of all, missing or outlier value control was performed during the data processing process; it was observed that there were no missing or inconsistent data sets. Since all attributes were numerical, no categorical coding or transformation was required. In addition, since the tree-based models used were insensitive to data scaling, normalization or standardization processes were not applied (Siddique et al., 2025). The data set was randomly divided into 80% training and 20% test, and this separation was kept constant in all modelling processes. To assess potential multicollinearity among the input variables, a Variance Inflation Factor (VIF) analysis was performed. The computed VIF values were 10.31 for pH, 15.87 for activated carbon dosage (g/L), 28.18 for initial RhB concentration (mg/L), 2.66 for contact time (min), and 13.02 for adsorption capacity (mg/g). Although several predictors exhibited VIF values above the conventional threshold of 10, all variables were retained because the machine learning models employed in this study (Random Forest, XGBoost, CatBoost, and Gradient Boosting) are tree-based algorithms that do not assume linear independence among predictors and are known to be robust against multicollinearity.

2.5.3 *Machine Learning Models*

Four different regression algorithms were used to estimate the removal efficiency: Random Forest Regressor, XGBoost Regressor, CatBoost Regressor and Gradient Boosting Regressor. These algorithms are frequently preferred methods in the literature in terms of their ability to model nonlinear structures, high generalization performance and interpretability. Hyperparameter optimization for each model was performed with five-fold cross-validation using the GridSearchCV method. Model performances were evaluated comparatively with R^2 (coefficient of determination), RMSE (root mean square error) and MAE (mean absolute error) values calculated separately on the training and test data sets.

To evaluate the predictive performance of the machine learning models, several statistical indicators were employed to capture their accuracy, bias, and error magnitude. Among these, the Coefficient of Determination (R^2) was used to quantify the proportion of variance in adsorption efficiency that is explained by the model predictions. It is computed as shown in Eq. (3) and has been widely used in adsorption modelling studies to assess model goodness-of-fit (Li et al., 2025a, 2025b; Xie et al., 2025):

$$R^2 = 1 - \frac{\sum_{i=1}^{n}(y_i - \hat{y}_i)^2}{\sum_{i=1}^{n}(y_i - \bar{y})^2} \tag{3}$$

where y_i represents the actual adsorption efficiency, $\hat{y}_i$ denotes the predicted value, and $\bar{y}$ is the mean of the observed values.

This metric provides a quantitative estimate of the magnitude of prediction errors made by the model. It reflects the square root of the average squared differences between observed and predicted values, thereby penalizing larger errors more heavily. RMSE is calculated according to Eq. (4) (Li et al., 2025a, 2025b; Xie et al., 2025; Zhao et al., 2022):

$$RMSE = \sqrt{\frac{1}{n}\sum_{i=1}^{n}(y_i - \hat{y}_i)^2} \quad (4)$$

where n is the total number of data points.

MAE quantifies the average magnitude of prediction errors in a model, without considering their direction. It represents the mean of the absolute differences between observed and predicted adsorption efficiencies, offering an intuitive measure of overall model accuracy. MAE is computed using Eq. (5) (Li et al., 2025a, 2025b; Xie et al., 2025):

$$MAE = \frac{1}{n}\sum_{i=1}^{n}\left|y_i - \hat{y}_i\right| \quad (5)$$

The predictive model that exhibited the highest coefficient of determination (R^2) alongside the lowest root mean squared error (RMSE) was designated as the optimal model in terms of performance. In addition, a feature importance analysis was carried out to determine the key variables influencing RhB dye adsorption, thereby providing meaningful insights into the dominant factors and mechanisms driving the adsorption process.

To provide a clear overview of the modelling sequence, the complete machine learning workflow adopted in this study is summarised in Fig. 1, covering data pre-processing, model training and optimization, cross-validation, interpretability analyses (SHAP and PDP), and final model evaluation.

2.5.4 Model Explainability and Visualization Techniques

It was aimed not only to achieve high accuracy, but also to make model decisions transparent and interpretable. For this purpose, the contributions of the features on the model were evaluated using the SHAP (SHapley Additive exPlanations) algorithm (Abekoon et al., 2025; Ghafarian et al., 2022). The most effective variables were visualized with both the overall contribution (mean absolute SHAP value) and sample-based effects (beeswarm plot, dependence plot). In addition, the independent effects of variables on the target variable were examined in detail with Partial Dependence Plot (PDP) analyses. Interactions between attributes were determined with SHAP interaction values analyses and interaction matrices were created. The learning behaviour of the model was evaluated with train-test learning curves; the structure of model errors was examined with residual analyses (Tedoldi et al., 2025).

The present study did not include an external or independent validation dataset due to the absence of compatible published data for this specific experimental design. Although the expanded dataset (n = 110) improves model stability, the lack of external validation remains a methodological limitation. Future studies should incorporate independent datasets or multi-laboratory measurements and explore larger data-driven frameworks to further evaluate and strengthen model generalizability.

3 Results and Discussion

3.1 Structural and Surface Characterization of the Biochar

3.1.1 Surface Morphology (SEM Analysis)

The surface properties of adsorbent materials are the basic parameters that directly affect the adsorption capacity and mechanism. Therefore, scanning electron microscopy (SEM) analysis was performed to evaluate the surface morphology of the synthesized *Ulva lactuca – Cystoseira sl.* based composite material. SEM images enable the surface structure of the material to be observed at high resolution, allowing the determination of critical morphological properties such as pore size, shape, surface roughness and particle distribution. In addition, by comparing the surface changes before and after adsorption, direct information can be obtained about the level of interaction of the pollutants with the surface and the success of adsorption (Wang et al., 2023). In this context, SEM analysis is a very valuable characterization method in terms of verifying both the structural integrity and functional efficiency of the adsorbent.

As shown in Fig. 2, the composite surface before adsorption exhibits a rough, porous, and irregular morphology consistent with its high BET surface area (797.91 m^2/g) (Ahmad & Rahman, 2011). The pristine adsorbent also displays a heterogeneous pore structure with pronounced textural irregularities and observable interparticle voids. Such heterogeneous and hierarchical pore architectures are characteristic of high-efficiency carbonaceous adsorbents and are known to enhance intraparticle diffusion and overall

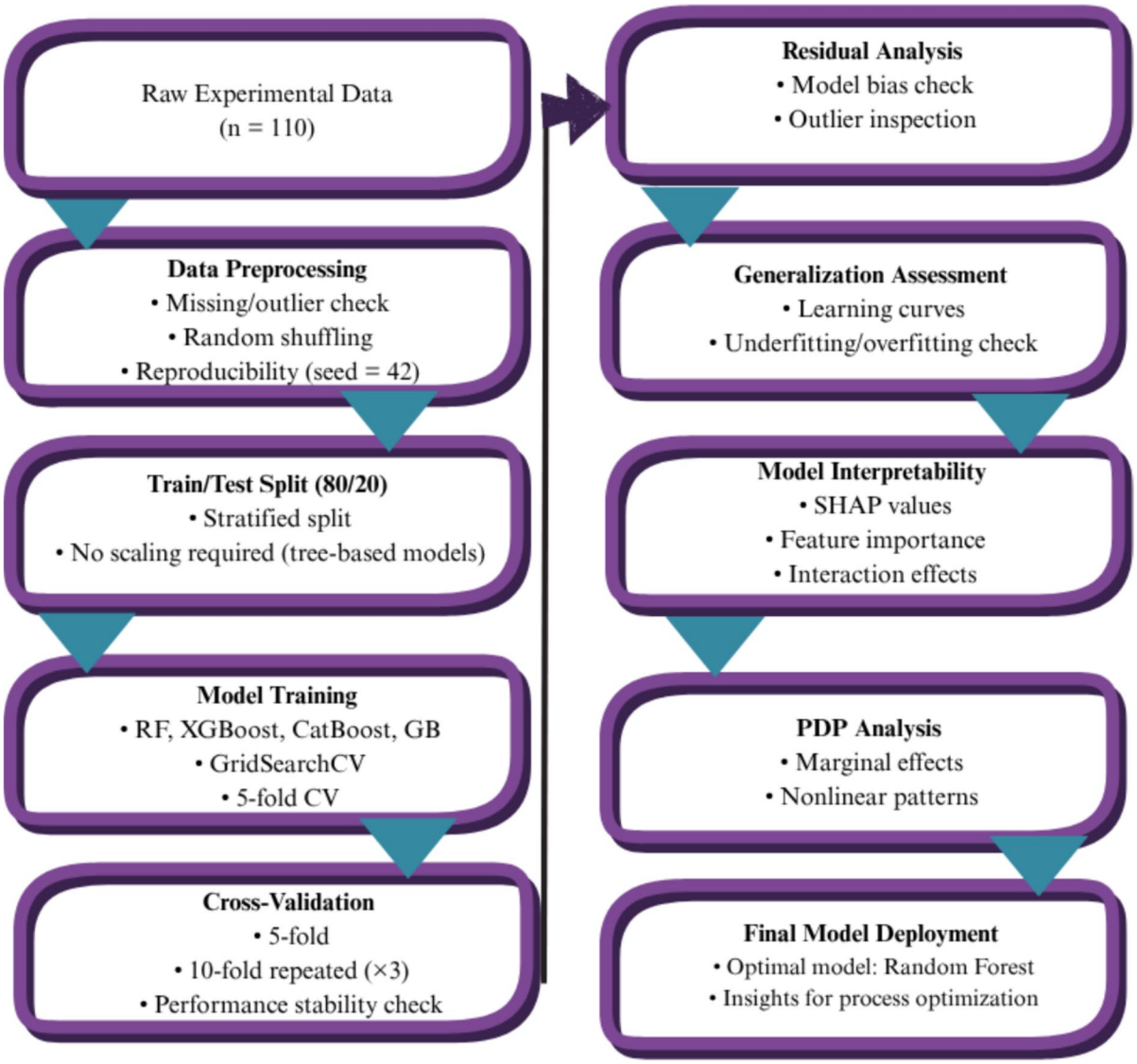

Fig. 1 Workflow diagram summarizing the machine learning steps used in this study

mass-transfer performance during dye removal (Li et al., 2023). In contrast, the SEM images obtained after adsorption show a noticeably smoother surface with partially filled or collapsed pores, indicating substantial morphological alteration upon dye uptake (Bhatnagar & Sillanpää, 2010). The loss of well-defined pore boundaries and the appearance of condensed surface regions suggest that Rhodamine B molecules accumulate not only on the external surface but also within internal pore channels, contributing to structural compaction (Ma et al., 2023). This behaviour is consistent with typical retention mechanisms of organic dyes on carbon-based materials (Gupta & Suhas, 2009). The post-adsorption micrographs further reveal particle accumulation and clear pore blockage, supporting the occurrence of physicochemical interactions between the adsorbent's active sites and the dye molecules (Ho & McKay, 1999). Additionally, the observed smoothing of surface asperities, reduction in accessible pore volume, and formation of dye-associated aggregates provide morphological evidence for π–π interactions, electrostatic

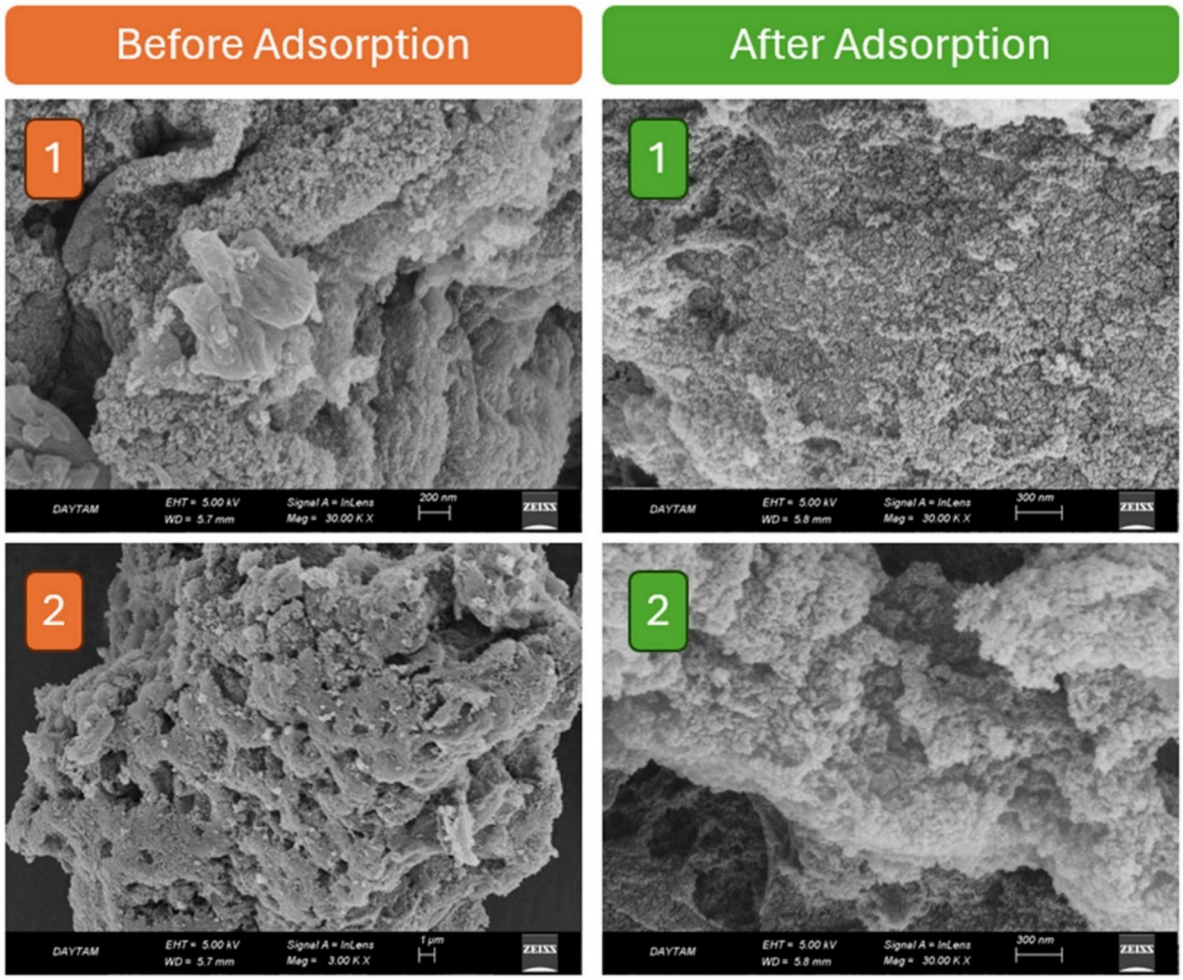

Fig. 2 SEM morphological characterization of the composite adsorbent before and after adsorption

attractions, and hydrogen bonding-mechanisms frequently proposed for Rhodamine B adsorption onto carbonaceous materials (Li et al., 2023). These findings also align with the gradual decline in adsorption capacity observed in reusability tests, as irreversible dye deposition and partial pore obstruction hinder the complete regeneration of the original surface structure (Foo & Hameed, 2012; Su et al., 2022).

As shown in Fig. 3, the EDX spectra before and after adsorption reveal clear changes in the elemental composition of the composite. Prior to adsorption, the surface is mainly characterized by strong C and O signals typical of biochar-based materials. After adsorption, the appearance and increase of the nitrogen (N K) peak indicate the successful deposition of Rhodamine B molecules on the adsorbent surface, as RhB contains nitrogen-bearing functional groups. Minor variations in P and K signals also suggest subtle surface chemistry modifications following dye uptake. These results confirm that the dye is effectively immobilized on the composite surface, supporting the SEM and FTIR findings.

3.1.2 Surface Chemistry (FTIR Analysis)

Fourier Transform Infrared Spectroscopy (FTIR) analysis was performed to determine the functional groups of the adsorbent and possible interaction mechanisms with Rhodamine B. The changes in the characteristic bands indicate possible bonding and

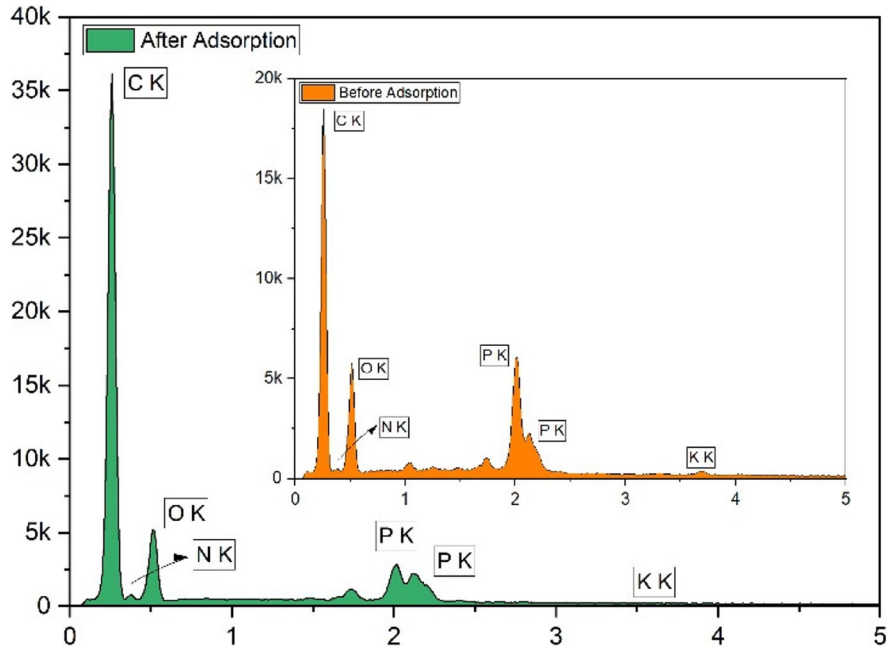

Fig. 3 EDX analysis of the composite adsorbent before and after dye adsorption

functional group participation in the surface chemistry after the adsorption process (Salleh et al., 2011).

When the FTIR spectra are examined, the broad band observed in the pre-adsorption spectrum (blue curve) in the region of 3400–3200 cm^{-1} corresponds to O–H stretching vibrations (Fig. 4). The band around 1700–1600 cm^{-1} indicates C = O stretching. In addition, the peaks in the range of 1100–1000 cm^{-1} indicate the presence of C–O or P–O groups. These functional groups are typical of biochar surfaces and are known to serve as active sites for pollutant immobilization through hydrogen bonding and electrostatic interactions (Behera et al., 2024).

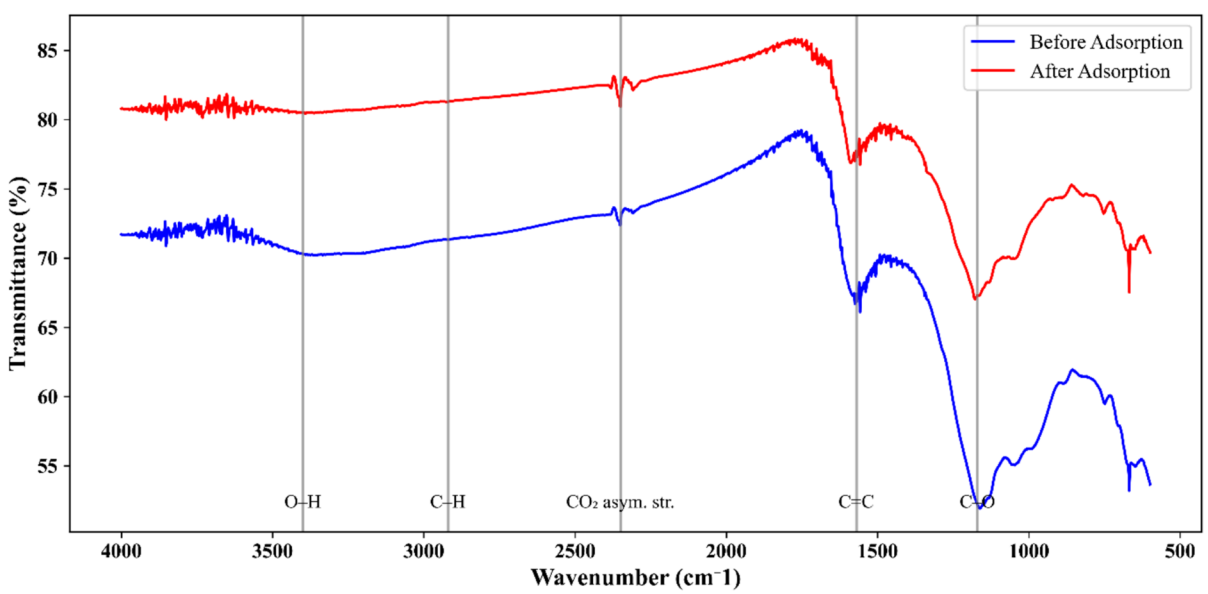

Fig. 4 FTIR spectra of the composite adsorbent before and after adsorption

In the post-adsorption spectrum (red curve), a decrease, displacement or shift in the intensity of these characteristic peaks was observed (Fig. 4). This situation shows that Rhodamine B molecules interact with the hydroxyl, carbonyl and phosphate groups on the surface, causing changes in the surface chemistry (Rafatullah et al., 2010). The decreases in the peak intensities support that especially the active groups are bound with the pollutant and chemical adsorption occurs in these regions (Crini & Badot, 2008). Additionally, slight shifts in the aromatic-related bands may suggest π–π interactions between the aromatic rings of Rhodamine B and the conjugated domains of the biochar surface, a mechanism commonly reported for aromatic dye adsorption (Fu et al., 2015). These results show that the FTIR analysis confirms that the adsorption mechanism occurs through the functional groups on the surface and that physicochemical interactions are involved in the process.

3.1.3 Porosity and Surface Area (BET Analysis)

Multi-point BET analysis was performed to determine the surface area and pore structure of the composite adsorbent. This analysis provides quantitative data on the specific surface area and adsorption behaviour of the material, allowing the characterization of porous structures.

The isotherm curve shown in Fig. 5a shows that the adsorption volume increases with increasing relative pressure and that the surface can adsorb a significant amount of gas. The obtained isotherm shows closeness to the Type IV isotherm behaviour, indicating a mesoporous structure. The graph given in Fig. 5b was created using the classical BET equation. Although the graph does not show linear character, surface area calculations were made by evaluating it in a certain relative pressure range (P/Po ≈ 0.05–0.3). The high surface area value obtained (797.91 m^2/g) supports the porous structure observed in SEM images and shows that the composite can effectively adsorb pollutants such as Rhodamine B (Crini & Badot, 2008).

The pore size distribution (PSD) of the activated carbon, obtained using non-local density functional theory (NLDFT) applied to the N_2 adsorption isotherm, is shown in Fig. 6. The material exhibits a pronounced peak in the micropore region (pore width < 20 Å), indicating that the carbon is predominantly microporous. The sharp maximum cantered at approximately 10–12 Å suggests the presence of well-developed ultra micropores and supermicropores, which typically arise from narrow slit-shaped pores generated during the carbonization and activation processes. Beyond the main micropore peak, the PSD displays a continuous decrease in pore volume extending into the mesopore range (20–50 Å). The gradual decline in mesopore volume and absence of any secondary mesopore maximum indicate that mesoporosity is present but not strongly developed. This behaviour is characteristic of activated carbons produced under conditions that favour the widening of micropores rather than the formation of distinct mesoporous networks. The overall PSD shape suggests that the accessible pore structure is dominated by narrow micropores that contribute significantly to the total pore volume and surface area. Such a distribution is advantageous for applications requiring high adsorption affinity and strong confinement effect, including the adsorption of small organic molecules. Overall, the NLDFT results confirm that the activated carbon exhibits a typical micropore-rich structure with a modest contribution from wider mesopores, consistent with materials produced through chemical activation routes emphasizing high surface area and narrow pore development. Moreover, previous studies have reported that micropore-rich activated carbons exhibit high dye adsorption capacities and strong adsorption affinity due to their narrow pore structures (Jawad et al., 2021).

3.2 Adsorption Behaviour under Varying Conditions

3.2.1 Effect of Solution pH and pH_{pzc} Determination

In order to determine the surface charge characteristics of the composite adsorbent, pH_{pzc} (zero charge point) analysis was performed. This analysis determines at which pH value the surface of the adsorbent remains neutral, contributing to the evaluation of electrochemical effects on surface-pollutant interactions.

As seen in the graph, the ΔpH value also increases regularly with the increase in the initial pH value. This shows that the adsorbent surface becomes protonated (positively charged) at low pH conditions and deprotonated (negatively charged) at high pH conditions (Li et al., 2012). The pH value at which ΔpH is closest to zero is determined as approximately 4.0,

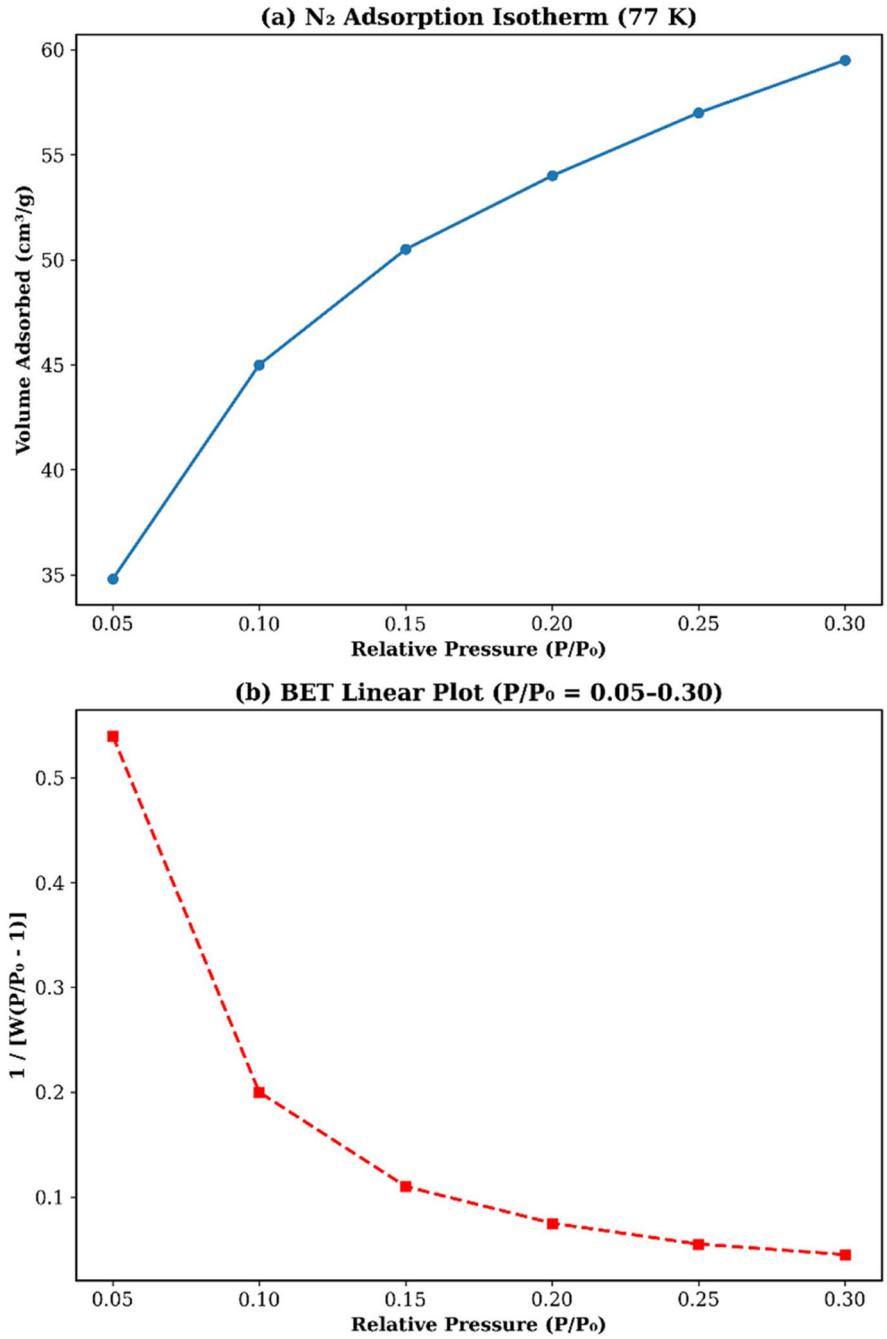

Fig. 5 BET surface analysis of the composite biochar. **a** Nitrogen adsorption–desorption isotherm used to evaluate the textural properties of the material. **b** BET linear plot employed for the determination of specific surface area

and this point is defined as pH_{pzc} where the surface charge of the adsorbent is neutral (Fig. 7). This result shows that the adsorption behaviour changes depending on pH and that ionic interactions play an important role (Foo & Hameed, 2010). Especially at pH values below pH_{pzc}, the positive charge of the surface can facilitate more effective adsorption of anionic species (Tang et al., 2014).

The pH value of the solution is one of the most important parameters affecting the adsorption efficiency. Therefore, Rhodamine B removal performance at different pH conditions was evaluated on

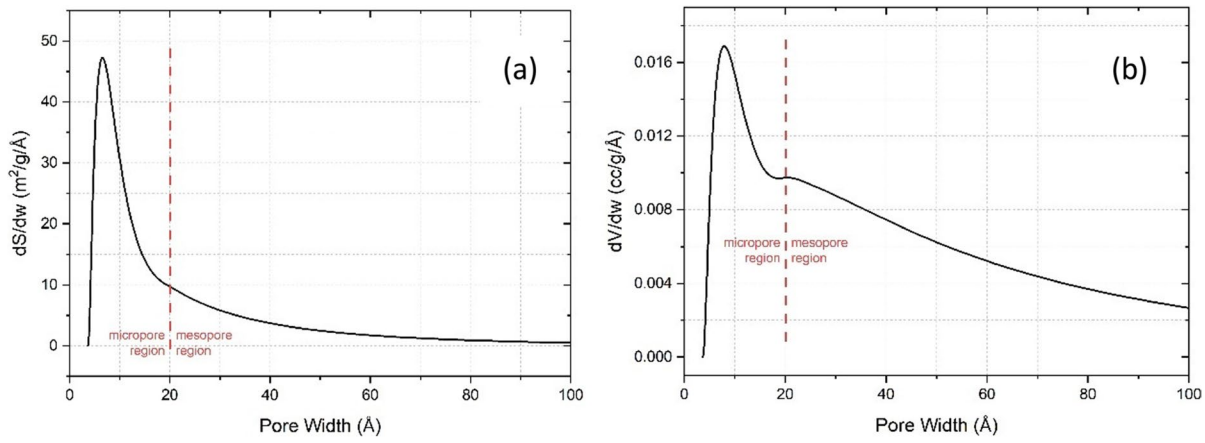

Fig. 6 Pore size distribution (PSD) of the activated carbon calculated from NLDFT studies. **a** Surface Area Pore Size Distribution **b** Pore Volume Distribution

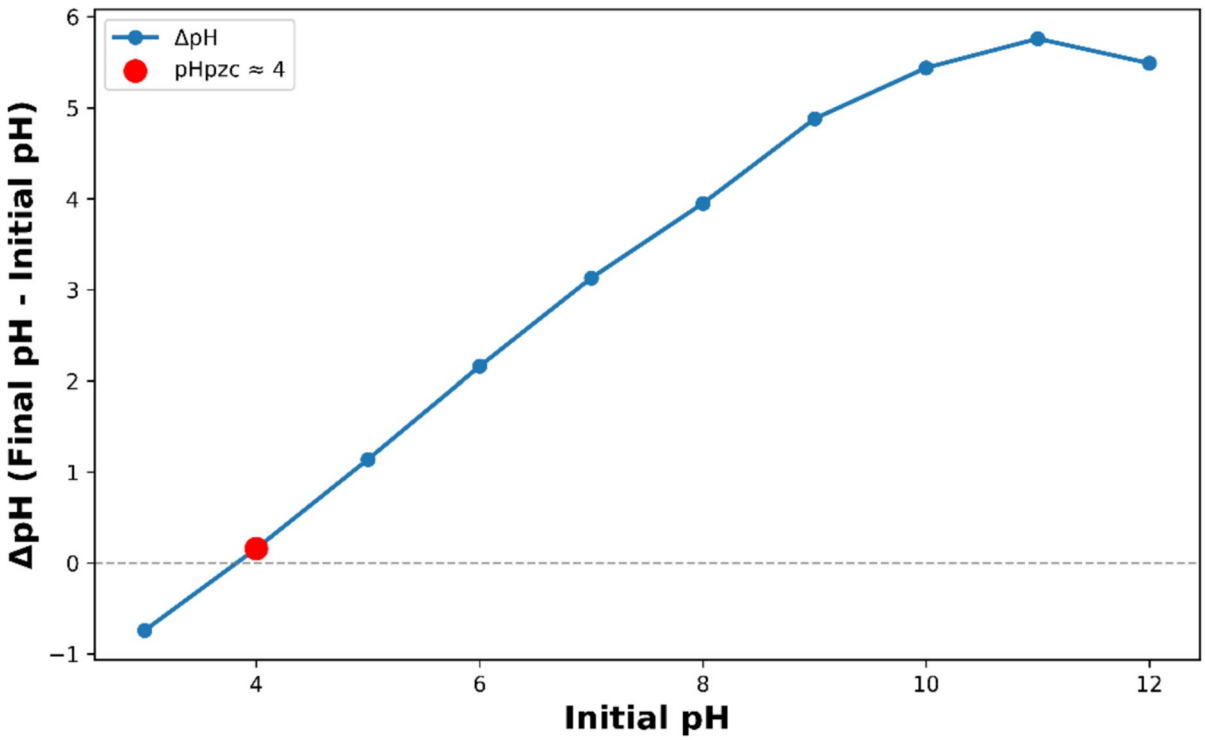

Fig. 7 Variation of ΔpH (Final pH – Initial pH) as a function of initial pH

a time basis and both removal efficiency (%) and adsorption capacity (mg/g) were determined.

According to Fig. 8a, rapid removal occurred in the first min of adsorption and as time progressed, the system reached equilibrium. Removal efficiency increased with increasing time in all pH ranges, and maximum removal values were reached especially in the pH 6–8 range (over 99%). This shows that the composite adsorbent is effective in a wide pH range (Pompeu et al., 2023).

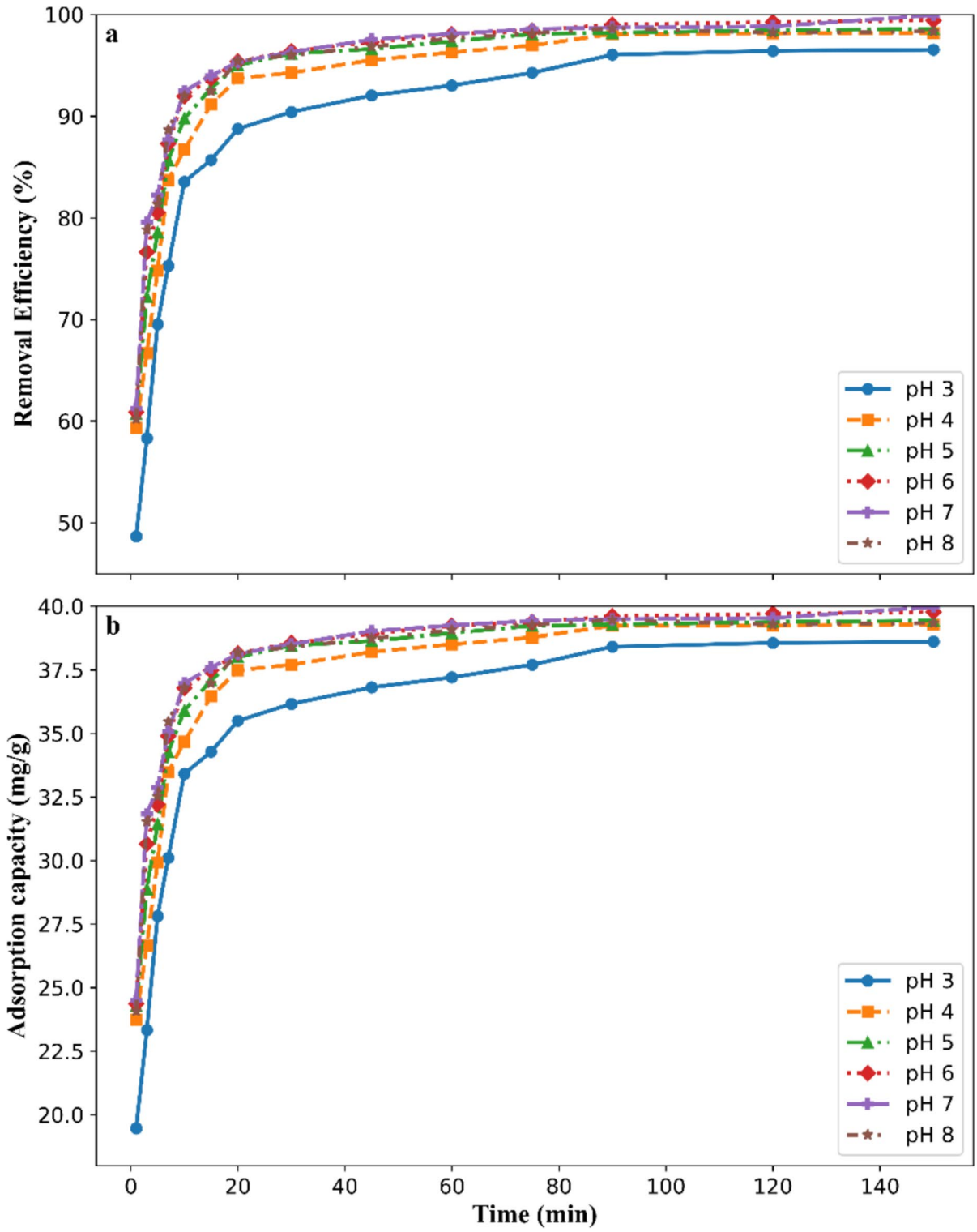

Fig. 8 Effect of pH on the time-dependent performance of Rhodamine B adsorption: **a** removal efficiency (%) an **b** adsorption capacity (qt, mg/g) (Experimental conditions: initial dye concentration (C_0) = 20 mg/L; adsorbent dosage = 0.5 g/L)

As seen in Fig. 8b, the adsorption capacity (q_t) also showed a similar trend. Especially at low pH value (pH 3), the adsorption of anionic dyes such as Rhodamine B was partially limited due to protonation of the surface (Crini, 2006). In the pH 6–7 range, the electrostatic interaction of the surface charge and the dye became more balanced and maximum capacity values were obtained (approximately 39 mg/g). These findings are also consistent with the pH_{pzc} value and show that the surface chemistry of the adsorbent interacts with the pollutant in a pH-sensitive manner.

3.2.2 *Effect of Biochar dosage*

The amount of adsorbent is a basic parameter that changes the adsorption efficiency by directly affecting the number of active sites in the system. Therefore, the effect of different adsorbent doses on the removal efficiency and adsorption capacity was evaluated.

According to Fig. 9, as the adsorbent dose increased, the removal efficiency increased significantly, almost reaching 99% at doses above 0.5 g/L. This increase can be explained by the formation of more active surface area and binding sites in the system (Ahmad & Alrozi, 2011). On the other hand, the adsorption capacity (mg/g) decreased with increasing adsorbent dose. This is related to the decrease in the load per unit adsorbent due to the distribution of a fixed amount of absorbable pollutant over a larger amount of adsorbent surface (saturation effect) (Hameed et al., 2007). In addition, the possibility of agglomeration between particles at high doses may prevent the effective use of the active surface. As a result, the optimum adsorbent dose should be determined to provide both maximum removal efficiency and high capacity (Crini & Badot, 2008).

3.2.3 *Effect of Initial Dye Concentration*

Initial concentration of pollutant in solution is an important factor affecting the adsorption kinetics and equilibrium state. Therefore, the effects of different initial Rhodamine B concentrations on the removal efficiency and adsorption capacity were investigated.

According to the graph (Fig. 10), as the initial concentration increases, the adsorption capacity (mg/g)

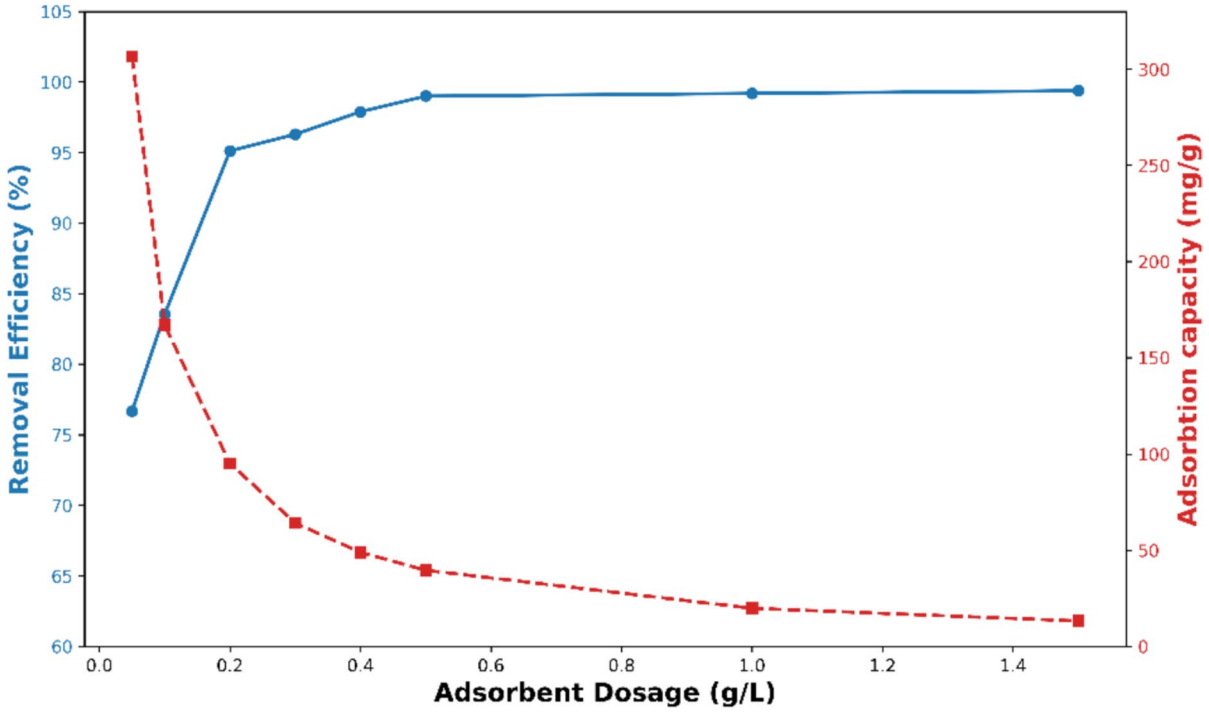

Fig. 9 Influence of biochar dosage on Rhodamine B removal efficiency and adsorption capacity (pH 6, $C_0 = 20$ mg/L, contact time = 90 min)

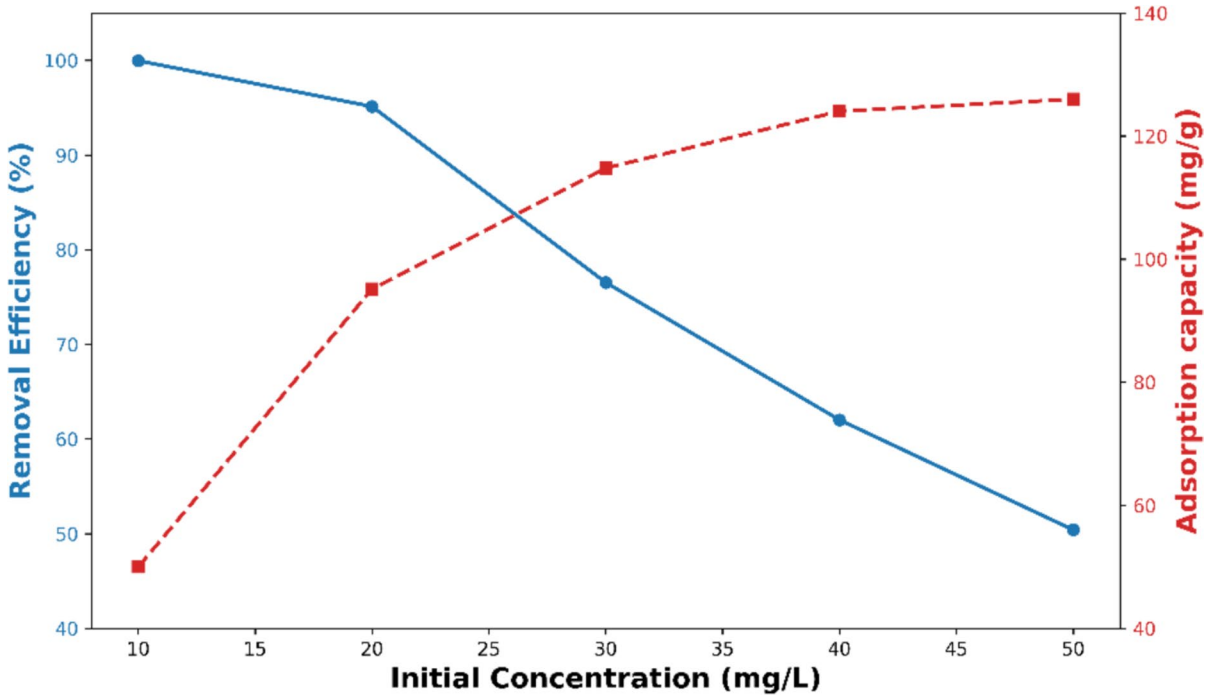

Fig. 10 Effect of initial Rhodamine B concentration on removal efficiency and adsorption capacity (adsorbent dose = 0.2 g/L, pH 6, contact time = 90 min)

increases significantly, while the removal efficiency decreases. At low concentrations (10–20 mg/L), both the capacity and removal efficiency are high due to the presence of sufficient active sites on the adsorbent surface.

However, as the initial concentration increases, surface saturation is reached since the adsorption sites remain relatively constant, which causes a decrease in the total removal efficiency (Foo & Hameed, 2010). High initial concentrations increase the diffusion resistance, leading to an increase in the amount of dye remaining in the solution. These findings reveal that the active sites on the surface remain limited under conditions exceeding the capacity of the system and that the efficiency decreases are related to the adsorption mechanism (Liu, 2008).

3.2.4 Reusability and Regeneration Potential

Reusability of an adsorbent is an important criterion for sustainable applications. Therefore, the capacity loss of the composite adsorbent during consecutive adsorption–desorption cycles was investigated and the performance change was evaluated.

As seen in Fig. 11, while the adsorption capacity was 95.12 mg/g in the first cycle, this value decreased to 76.23 mg/g in the fifth cycle. The gradual decrease observed in performance is most likely due to partial blockage of the active sites on the surface, structural deterioration or incomplete desorption (Baskar et al., 2022). Despite this, the preservation of over 80% capacity at the end of five cycles shows that the composite adsorbent has reusability and can be an economical alternative in practical applications (Gupta & Nayak, 2012).

3.3 Adsorption Kinetics and Isotherm Modelling

3.3.1 Kinetic Analysis: Pseudo-First-Order vs. Pseudo-Second-Order

In order to better understand the adsorption kinetics of Rhodamine B (RhB) dye by composite biochar, two different kinetic models were applied to the experimental data obtained at different initial concentrations (10 and 20 mg/L). In this context, pseudo-first-order (PFO) and pseudo-second-order (PSO) kinetic models were evaluated and the adsorption rate

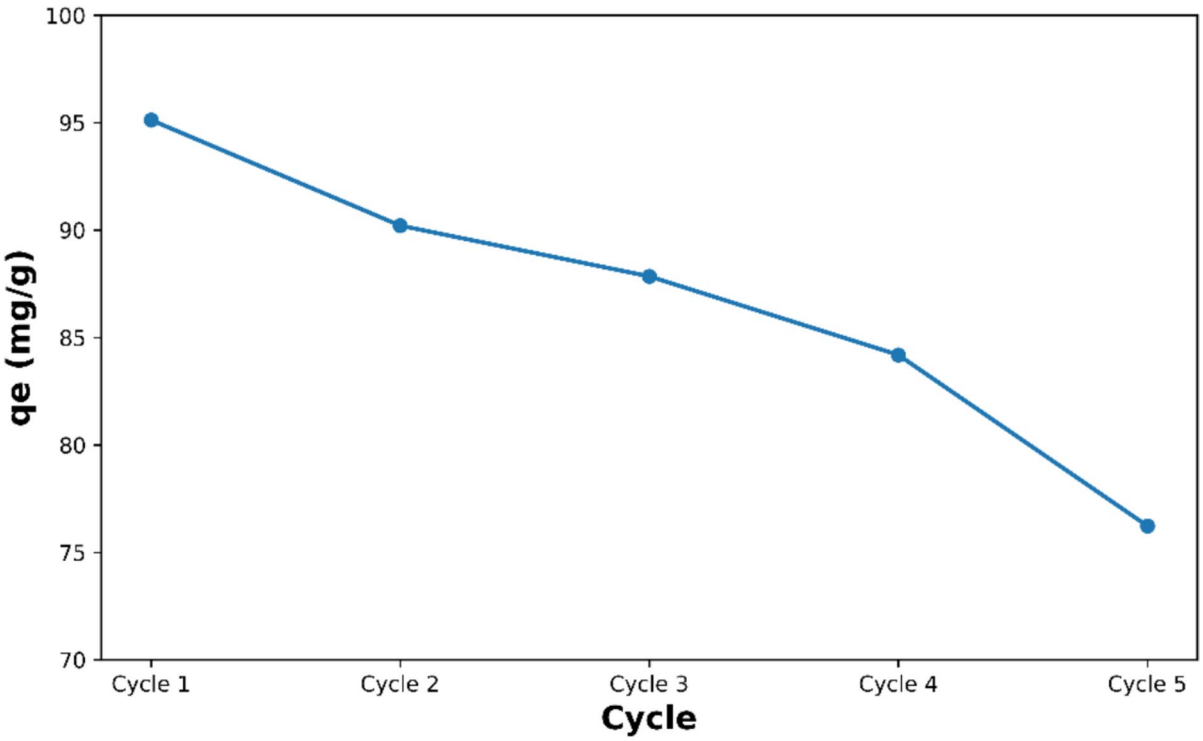

Fig. 11 Reusability of the adsorbent over successive adsorption–desorption cycles: adsorption capacity (qe, mg/g) after each cycle

constant, equilibrium capacity and degree of fit (R^2) were determined for each model.

When Fig. 12 is examined, it is seen that both models are compatible with the experimental data, but the PSO model stands out with a higher fit success. Especially at the initial concentrations of 10 mg/L and 20 mg/L, the curves of the PSO model reflect the adsorption tendencies more accurately. This suggests that the system operates with an adsorption mechanism based on chemical interactions. In addition, the fact that the system reaches equilibrium in the first 30 min reveals that the adsorbent surface has a high interaction potential against RhB molecules.

The kinetic parameters in Table 1 show that the PSO model gives the most compatible results with the experimental data with high R^2 values (0.993) at both concentration levels. In addition, it is seen that the q_e values obtained with the PSO model are closer to the experimental q_e. These findings support that the chemical bonding between the surface and the adsorbed molecule is effective in the adsorption process and that the PSO model is more successful in describing this system.

3.3.2 Equilibrium Isotherm Models: Langmuir vs. Freundlich

In order to investigate the adsorption behaviour in more detail, the obtained equilibrium data were applied to Langmuir and Freundlich isotherm models. With these models, the surface properties of the composite biochar, maximum adsorption capacity and the nature of the adsorbent-adsorbate interaction were evaluated.

As shown in Fig. 13, the Langmuir model predicts on the basis of a single-layered, homogeneous surface, while the Freundlich model describes multilayer adsorption on heterogeneous surfaces. When both models are examined graphically, it is clear that the Freundlich model more accurately represents the experimental data. This indicates that there are regions on the adsorbent surface that differ in energy and that multilayer adsorption is effective.

According to the isotherm parameters presented in Table 2, the Freundlich model showed a higher fit coefficient ($R^2 = 0.994$) compared to the Langmuir model. This result reveals that the adsorption is not

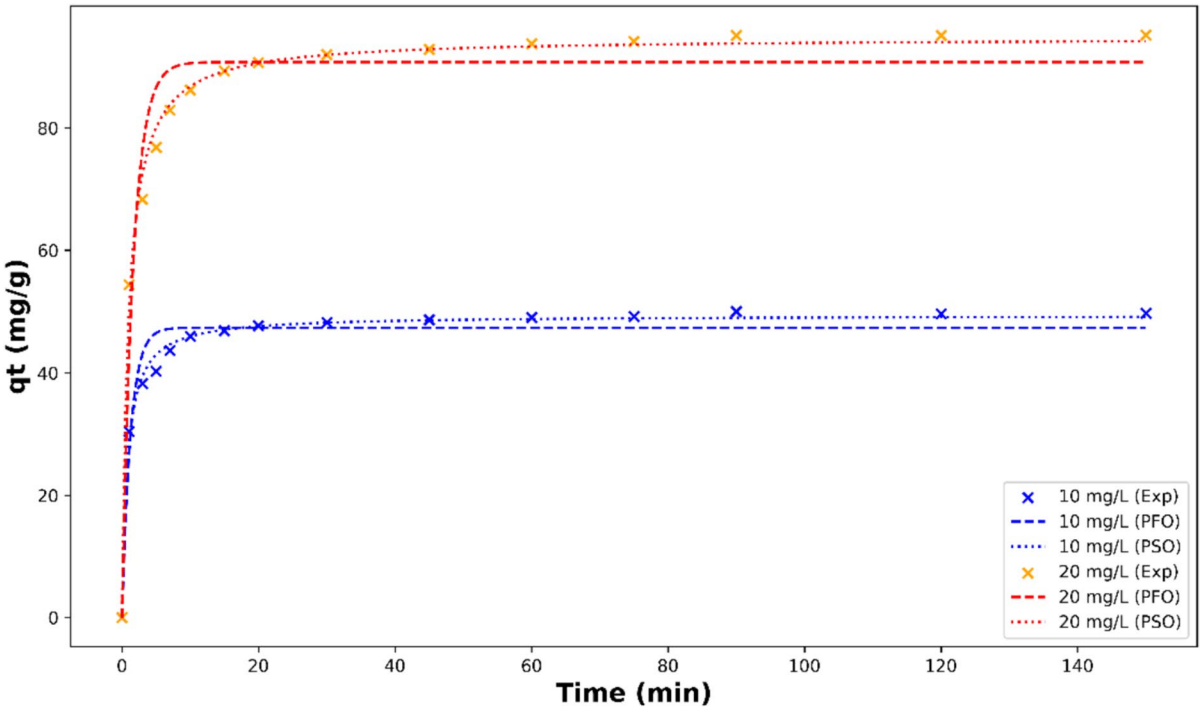

Fig. 12 Adsorption kinetics of RhB onto biochar (Temperature:25 °C; Initial RhB concentration: 10 and 20 mg/L; Biochar dose: 0.2 g/L; pH = 6)

Table 1 Kinetic parameters for RhB adsorbed onto composite biochar

Kinetic Models	Equation	Parameters	Biochar
Pseudo-first order (10 mg/L)	$q_t = q_e\left(1 - e^{-k_1 t}\right)$	q_e(mg/g)	47.3378
		k_1(min^{-1})	0.8019
		R^2	0.948
Pseudo-first order (20 mg/L)	$q_t = q_e\left(1 - e^{-k_1 t}\right)$	q_e(mg/g)	90.7733
		k_1(min^{-1})	0.6164
		R^2	0.948
Pseudo-second order (10 mg/L)	$q_t = \frac{k_2 q_e^2 t}{1+k_2 q_e^2 t}$	q_e(mg/g)	49.3730
		k_2(min^{-1})	0.0270
		R^2	0.993
Pseudo-second order (20 mg/L)	$q_t = \frac{k_2 q_e^2 t}{1+k_2 q_e^2 t}$	q_e(mg/g)	94.7644
		k_2(min^{-1})	0.0115
		R^2	0.993

limited to a homogeneous surface; on the contrary, the active sites on the surface are heterogeneous and multilayer interactions are dominant. In addition, high K_F and low n^{-1} values indicate that the system exhibits a strong adsorption tendency.

The fact that the Freundlich isotherm model provided the best fit for UCAC indicates the heterogeneous nature of its surface and the presence of energetically diverse active sites that facilitate multilayer adsorption. The pore structure developed during the activation process further reinforces this behaviour by generating regions with varying binding affinities. A comparative summary of UCAC's performance with previously reported biochar-based adsorbents is presented in Table 3. Notably, the maximum adsorption capacity of 126 mg/g obtained at an initial Rhodamine B concentration of 50 mg/L aligns with the upper segment of the broad performance range reported for biochar-type materials (5.6–190 mg/g), demonstrating the competitive adsorption capability of UCAC.

In addition to this favourable performance, many biochar's reported in the literature require energy-intensive synthesis conditions, extended activation times, or the use of multiple chemicals, all of which increase environmental burden and operational cost. In contrast, UCAC achieves comparable or superior adsorption capacities through a simpler activation strategy that demands lower energy input and minimal chemical usage. This production route substantially

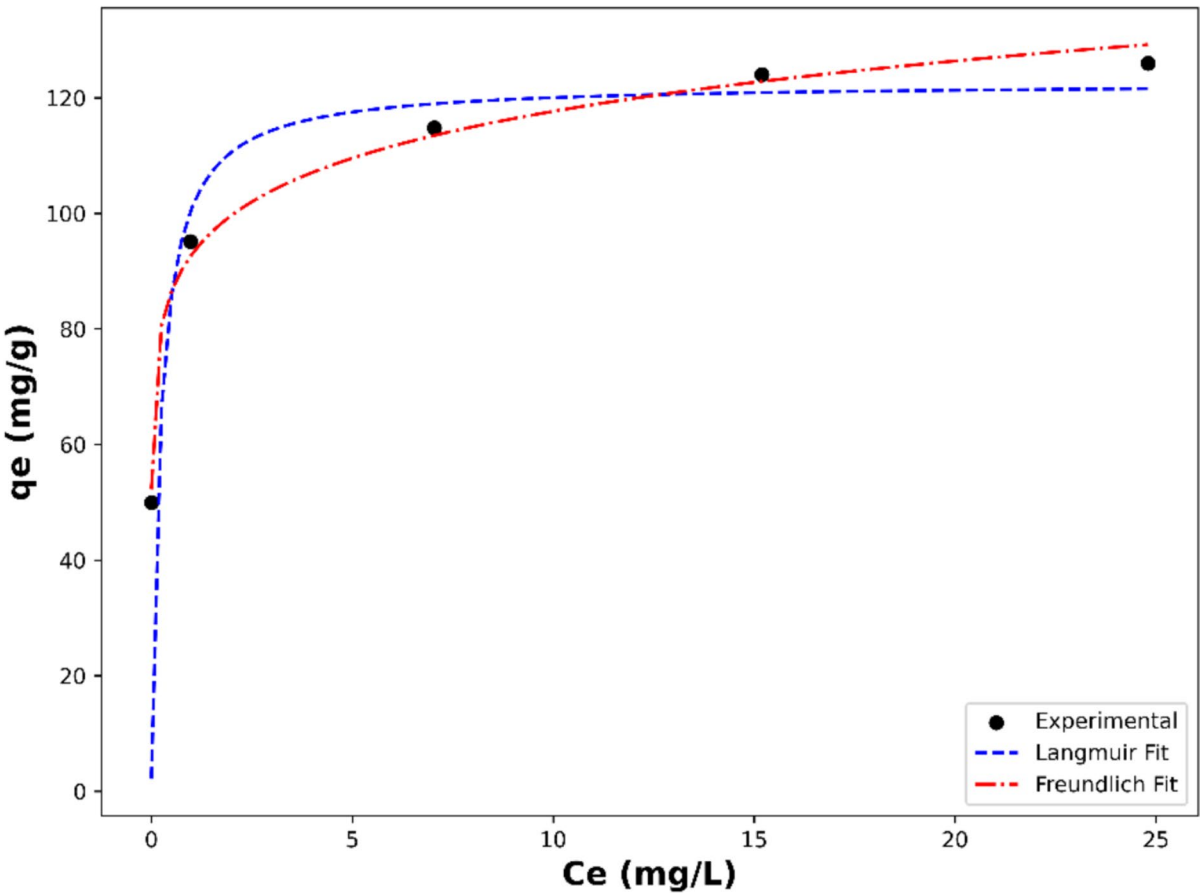

Fig. 13 Adsorption isotherms of RhB onto biochar (Temperature:25 °C; Biochar dose: 0.2 g/L for contact time: 90 min; pH = 6)

Table 2 Isotherm parameters for RhB adsorbed onto composite biochar

Isotherms model	Equation	Parameters	Biochar
Langmuir	$q_e = \frac{q_m K_L C_e}{1+K_L C_e}$	q_m(mg/g)	122.63888
		K_L(min^{-1})	4.612144
		R^2	0.40570
Freundlich	$q_e = K_F C_e^{1/n}$	K_F(g^{-1})	92.790140
		n^{-1}	9.694447
		R^2	0.99364

enhances its practical applicability. Furthermore, the utilization of rapidly renewable marine macroalgal biomass differentiates UCAC from numerous agricultural or lignocellulosic-based adsorbents, offering a more sustainable feedstock alternative. Taken together, these findings confirm that UCAC delivers an efficient adsorption performance for RhB removal while simultaneously offering environmental and operational advantages. Its combination of structural features, functional behaviour, and sustainable production approach positions UCAC as a strong alternative to conventional biochar adsorbents reported in the literature.

3.4 Machine Learning Model Performance and Interpretation

3.4.1 Predictive Model Comparison and Selection

To systematically assess the predictive capabilities of various machine learning algorithms, the estimated and observed values of "Removal Efficiency (%)" were comparatively analysed across four prominent models: Random Forest, XGBoost, CatBoost, and Gradient Boosting. This comparative evaluation

Table 3 Comparison of UCAC with Literature-Reported Biochar's for RhB Adsorption

Adsorbent	q_{max} (mg/g)	Carbonization conditions	References
Stalk corn activated carbon	5.6	Phosphoric acid (1 N) in a ratio of 1:10 (w/w) was used as the activating reagent. firstly in 500 °C for 30 min and after that in 700 °C for 15 min	Mousavi et al., 2023
Manganese titanium oxide composite biochar	19.06	Hydrothermal synthesis method (48 h and the hydrothermal synthesis temperature was 160 °C)	Yang et al., 2023
Coconut fruit shell biochar	8.1	The coconut fruit shells were pyrolyzed at 500 °C (heating rate: 10 °C min − 1) for 4 h	Kapoor et al., 2024
Hydrochar pyrolysis using bamboo shoot shells	85.8	800 °C for 2 h under N_2 flow, ramping at 4 °C/min	Hou et al., 2019
Hydrothermal carbonization synthesis of cassava slag biochar	105.3	The sample was hydrothermally treated at 180 °C for 12 h	Wu et al., 2020
Biochar from agricultural waste pine nutshell	110.68	Pyrolysis in a muffle furnace at 600 °C for 2 h under a nitrogen flow of 0.15 mL/min, using NaOH as the activating agent	Atalay Eroğlu et al., 2025
Biochar from *Calophyllum inophyllum* seeds	169.5	Pyrolyzed in a fixed bed pyrolysis reactor between 773 and 873 K at 298 K/min	Behera et al., 2024
Biochar Derived from *Atropa belladonna* L., (ABL) ABL@ZnCl2 ABL@H3PO4	190.63 184.70	$ZnCl_2$ and H_3PO_4 were used as the activating reagents. The mixture was pyrolyzed at 500 °C under a N_2 flow for 2 h in a tube furnace with a heating rate of 5 °C/min	Li et al., 2023
Biochar Derived from Marine Biomass	126	Pyrolysis in a microwave oven (700 W) for a total of 18 min divided into three cycles of 6 min	This study

enabled a comprehensive understanding of each model's performance in capturing the underlying patterns in the data.

The model comparison indicates that the Random Forest algorithm provides the most balanced and reliable overall performance, as shown in Fig. 14a. With the highest test R^2 value (0.93) and the lowest test RMSE (4.15) and MAE (1.95), the model demonstrates strong generalization capability without signs of overfitting. The corresponding numerical values are provided in Table 4.

Although XGBoost (Fig. 14b) maintained near-perfect performance on the training set, its higher test MAE (2.01) and comparable RMSE (4.20) indicate a mild overfitting tendency (Table 4). CatBoost (Fig. 14c) exhibited the most pronounced discrepancy between the training and test phases, confirming stronger overfitting behaviour, with a comparatively lower test R^2 (0.90) and the highest test errors (RMSE = 4.99; MAE = 2.76). Gradient Boosting (Fig. 14d), despite achieving an excellent fit on the training data, produced weaker test-set predictions (Test $R^2 = 0.90$; RMSE = 4.85), suggesting limited generalizability relative to Random Forest and XGBoost.

To better understand how reliably the Random Forest model generalizes to unseen data, both fivefold and tenfold cross-validation were applied. In the fivefold setting, the model showed noticeable variability, with an average R^2 of 0.748 and a relatively large standard deviation (± 0.366). This fluctuation is expected, given that each fold contains fewer samples, making the model more sensitive to data distribution. When the number of folds was increased to 10, the results became much more consistent. The mean R^2 rose to 0.919, and the standard deviation dropped markedly to ± 0.064, indicating a steadier predictive behaviour. The error metrics also improved, with RMSE decreasing from 4.55 to 2.54 and MAE from 2.37 to 1.59. Taken together,

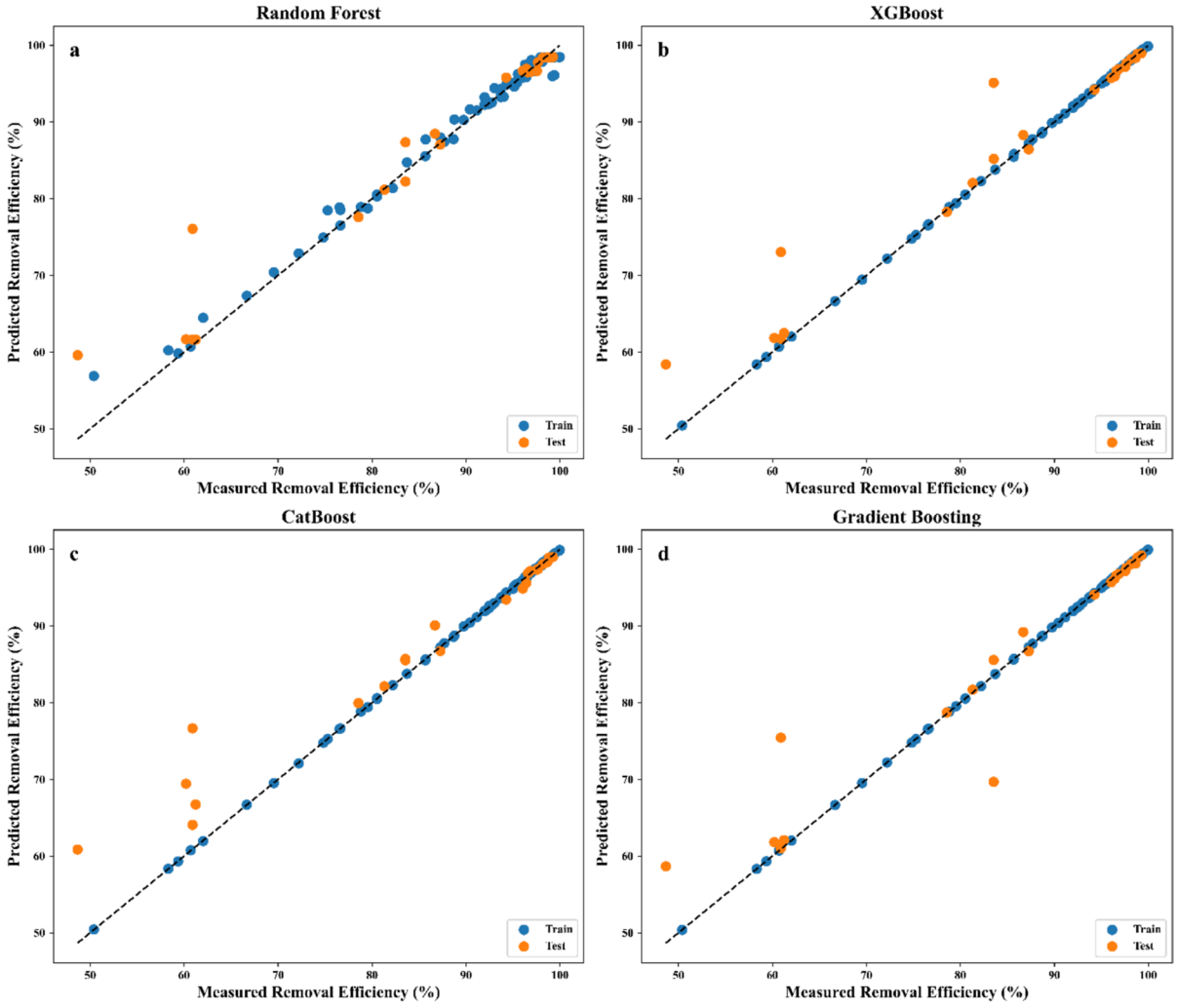

Fig. 14 Comparison of actual and predicted removal efficiency (%) values for the Random Forest **a**, XGBoost **b**, CatBoost **c**, and Gradient Boosting **d** models

Table 4 Model performance for ML models

Model	Data Set	R^2	RMSE	MAE
XGBoost	Training	0.99	0.07	0.06
	Test	0.93	4.2	2.01
Random Forest	Training	0.99	1.22	0.76
	Test	0.93	4.15	1.95
CatBoost	Training	0.99	0.07	0.06
	Test	0.90	4.99	2.76
Gradient Boosting	Training	0.99	0.03	0.02
	Test	0.90	4.85	2.21

these results show that the Random Forest model performs more stably under tenfold cross-validation and has strong potential for reliable generalization.

Figure 14a illustrates the performance of the Random Forest model, which shows the most balanced behaviour between the training and test sets, with predictions closely following the ideal 1:1 line despite moderate dispersion at lower efficiency levels. Figure 14b presents the XGBoost model, which achieves highly accurate predictions for both datasets, although a noticeable increase in prediction error appears in the mid-efficiency range, suggesting slight overfitting. Figure 14c displays the CatBoost model, which fits the training data almost perfectly

but deviates substantially in the test set, especially at lower removal efficiencies, indicating a pronounced overfitting tendency. In Fig. 14d, the Gradient Boosting model demonstrates consistent performance on the training set but weaker generalization on unseen data, as evidenced by higher test errors. Taken together, Fig. 14a–d show that Random Forest is the most stable and generalizable model, while XGBoost remains a competitive alternative with a greater susceptibility to overfitting. CatBoost and Gradient Boosting, despite their strong training accuracy, display comparatively weaker performance on the test dataset.

3.4.2 Feature Importance Analysis via SHAP Values

In addition to improving the predictive power of machine learning models, it is also very important in environmental systems to transparently explain which inputs these predictions are based on. To this end, the decision mechanism of the Random Forset model developed using the SHAP (SHapley Additive exPlanations) analysis method has been made interpretable. SHAP analysis quantitatively presents the contribution of each input to the target variable in terms of both direction (positive/negative effect) and magnitude. In this regard, SHAP provides much more detailed and reliable insights compared to classical importance analysis (Lundberg et al., 2020).

Figure 15 presents the SHAP (SHapley Additive exPlanations) summary bar plot, which illustrates the average impact of each input variable on the prediction of Rhodamine B (RhB) removal efficiency. Among the five evaluated features, contact time (min) emerges as the most influential parameter, with a mean absolute SHAP value of + 5.70. This indicates that longer contact durations substantially enhance removal performance by increasing the effective interaction between dye molecules and the adsorbent surface. The second most impactful factor is adsorption capacity (mg/g), with a SHAP value of + 2.39, highlighting the critical importance of the adsorbent's intrinsic capability in determining the removal performance.

Initial RhB concentration (mg/L) ranks third (+ 1.11), indicating a moderate yet meaningful influence on model predictions due to its effect on adsorption kinetics and saturation patterns. The contribution of pH (+ 0.30) is comparatively smaller, reflecting its secondary but still relevant role in modifying surface charge characteristics and dye ionization behaviour. Finally, biochar dose (g/L) exhibits the lowest SHAP contribution (+ 0.01), suggesting a minimal effect within the operational domain studied.

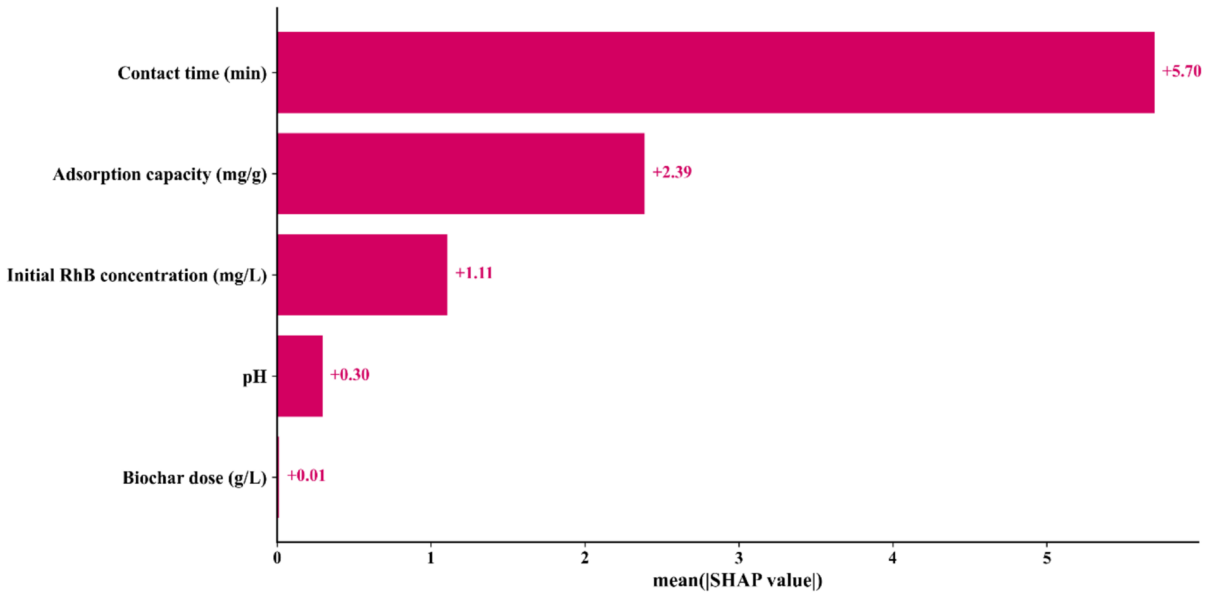

Fig. 15 Ranking of the five most important inputs based on average SHAP values. Quantitative axis labels were added to enhance interpretability

Overall, the SHAP analysis confirms that contact time and adsorption capacity are the dominant drivers of RhB removal efficiency in the Random Forest model, while other parameters contribute at lower magnitudes. These insights help clarify the underlying mechanisms governing the adsorption process and support improved optimization strategies.

Figure 16 displays the SHAP beeswarm plot, which provides a detailed visualization of how individual feature values influence the model's prediction of Rhodamine B (RhB) removal efficiency. Each point on the plot represents a single prediction for a given sample, coloured according to the magnitude of the feature value (from low in blue to high in red) and positioned along the x-axis based on its SHAP value, indicating its impact on the model output. Among the features, contact time (min) has the strongest and most consistent influence, with high contact time values (in red) generally pushing the prediction positively, while lower values (in blue) tend to reduce the predicted efficiency. This dominant effect is visible through the dense clustering of high-value points on the positive SHAP region. Adsorption capacity (mg/g) also exhibits a substantial positive contribution, particularly when higher values are present, indicating that adsorbents with greater capacity meaningfully increase model output. Compared with the previous interpretation, the effect appears even more distinct due to the tighter grouping of high-capacity values on the positive SHAP side. For initial RhB concentration (mg/L), higher concentrations show a mild positive influence, though the effect is more scattered and less dominant. pH demonstrates a weak and slightly positive impact, with some variability depending on the value range. Lastly, biochar dose (g/L) shows minimal SHAP variation, indicating a minimal role in shifting the model's prediction, regardless of its value. The extremely narrow spread of SHAP values along this feature confirms its limited role in the model's decision-making process.

Overall, this beeswarm plot reinforces the dominance of contact time and adsorption capacity while clarifying the relatively minor influences of pH, initial concentration, and adsorbent dosage. It complements the SHAP bar chart by illustrating not only which features are most important, but also how different magnitudes of feature values contribute asymmetrically to the prediction mechanism.

3.4.3 Partial Dependence Analysis of Key Variables

Partial Dependence Plot (PDP) analyses were performed to make the relationships between the model inputs and the predicted outputs more understandable. PDP graphs isolate the marginal effect of each variable on the model output, showing how the relevant variable behaves when all other variables are held constant (Ullah et al., 2023). This allows the direction

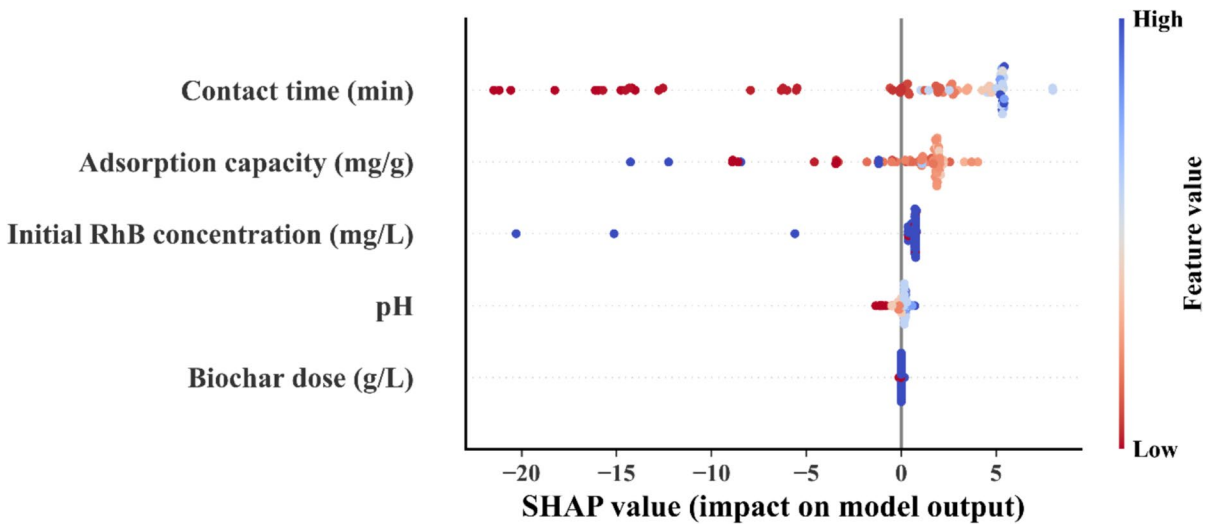

Fig. 16 SHAP beeswarm graph. The distribution of SHAP values highlights contact time and adsorption capacity as the dominant contributors to model predictions

of the model's decision mechanism and possible threshold behaviours to be more clearly revealed.

The PDP analyses in Fig. 17 are presented separately for the five variables determined to be the most important in the model. For the contact time (min) variable, the Random Forest PDP reveals a strong increase in predicted removal efficiency during the initial 20–30 min, followed by a more gradual rise

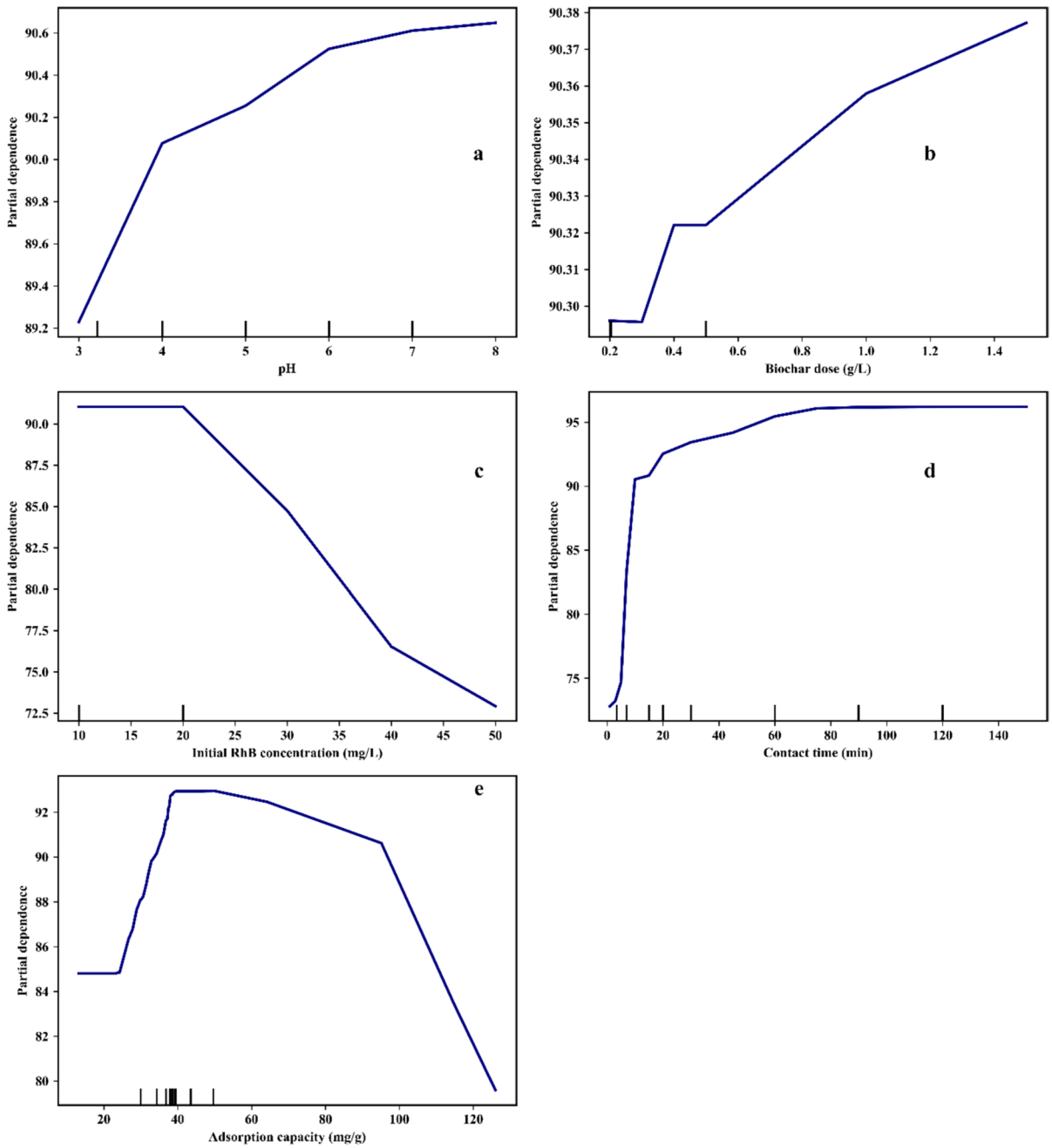

Fig. 17 PDP analyses for the four most important variables: **a** Contact time, **b** Initial RhB concentration, **c** Biochar dose, **d** pH, **e** Adsorption capacity. PDPs show that contact time increases removal efficiency, while higher initial RhB concentrations reduce it; other variables exhibit more moderate effects

until approximately 90–100 min. This trend is consistent with adsorption kinetics, where rapid initial uptake transitions into a slower diffusion-controlled phase as surface active sites become progressively occupied (Oliveira et al., 2023; Tomasella et al., 2025; Hu et al., 2018). This increase continues until approximately 80 min, after which the efficiency increase becomes horizontal. This situation can be explained by the surface reaching saturation and the onset of mass transfer limitations (Satayev et al., 2024; Hernández-Abreu et al., 2020). For adsorption capacity (mg/g), the PDP shows that efficiency increases sharply at moderate capacity levels (around 50–70 mg/g), but declines at very high values (> 110 mg/g). This nonlinear behaviour indicates that while higher capacities improve adsorption performance, extremely high values may introduce structural or transport limitations (Ozcan et al., 2024; Zhao et al., 2024). An inverse relationship was determined for the Initial RhB concentration (mg/L) variable. High removal efficiency is predicted at lower initial RhB concentrations, whereas efficiency progressively decreases as concentration increases. This finding shows that the adsorbent surfaces have limited active points and that reaching saturation of these points limits the efficiency (Alraae et al., 2025). The PDP for biochar dose (g/L) indicates a mild and steady increase in predicted efficiency across the tested range (0.2–1.5 g/L), without a clear saturation threshold. This suggests that although higher biochar doses contribute positively, their overall influence remains limited within the studied interval (Hashem et al., 2024; Ozcan et al., 2024). These analyses show that the model not only provides high predictive performance but also captures nonlinear patterns consistent with adsorption behaviour, thereby enhancing both model reliability and the interpretability of environmental processes.

3.4.4 SHAP-Based Interaction Effects among Features

Interpretability is as important as accuracy in machine learning models (Li et al., 2025a, 2025b). SHAP-based interaction analysis allows visualization of not only the contribution of a single feature to the model, but also its effect in interaction with other variables. With this method, it becomes clear how the model learns complex and nonlinear relationships (Esu et al., 2024).

Figure 18a–e presents the SHAP dependence plots that illustrate how the individual input features and their interactions with secondary variables influence the Gradient Boosting model's prediction of Rhodamine B (RhB) removal efficiency. In Fig. 18a, the SHAP value for pH increases steadily with rising pH levels, indicating a strong positive contribution to removal efficiency under more alkaline conditions. The colour gradient shows that longer contact times further amplify this effect, highlighting interaction between variables (Kumar et al., 2025; Zhang et al., 2025). Notably, longer contact times (indicated by warmer colours) further amplify this effect, suggesting a synergistic interaction. In Fig. 18b, the effect of biochar dose on model output is most significant at low dosages, where the SHAP values are relatively positive. As the dose increases, the marginal impact diminishes, possibly due to surface saturation or particle agglomeration (Arabzadeh Nosratabad et al., 2024). The updated plot clearly shows that increasing the dosage provides a positive but low-gradient contribution. Figure 18c displays the SHAP response for the initial RhB concentration (mg/L), where SHAP values shift markedly into the negative range at higher concentrations. This indicates that increasing the initial dye concentration reduces predicted efficiency, reflecting the rapid saturation of active adsorption sites. The updated graph shows that low concentration ranges provide more stable and positive model responses. In Fig. 18d, contact time emerges as a dominant driver of model predictions. SHAP values rise sharply during the first 20–30 min, followed by a clear plateau around 80–100 min, consistent with adsorption equilibrium behaviour. Figure 18e shows that higher adsorption capacities (mg/g) are generally associated with higher SHAP values, confirming that adsorbent quality significantly strengthens the model's confidence in predicting high removal efficiency. The updated plot indicates a strong increase at low–moderate capacities, followed by a decline at very high capacities, suggesting diminishing returns due to potential pore saturation or structural limitations. Collectively, these SHAP dependence plots confirm that the model's decision-making behaviour is physically interpretable and consistent with known adsorption mechanisms. The colour gradients further reveal meaningful interaction patterns-especially for contact time and adsorption

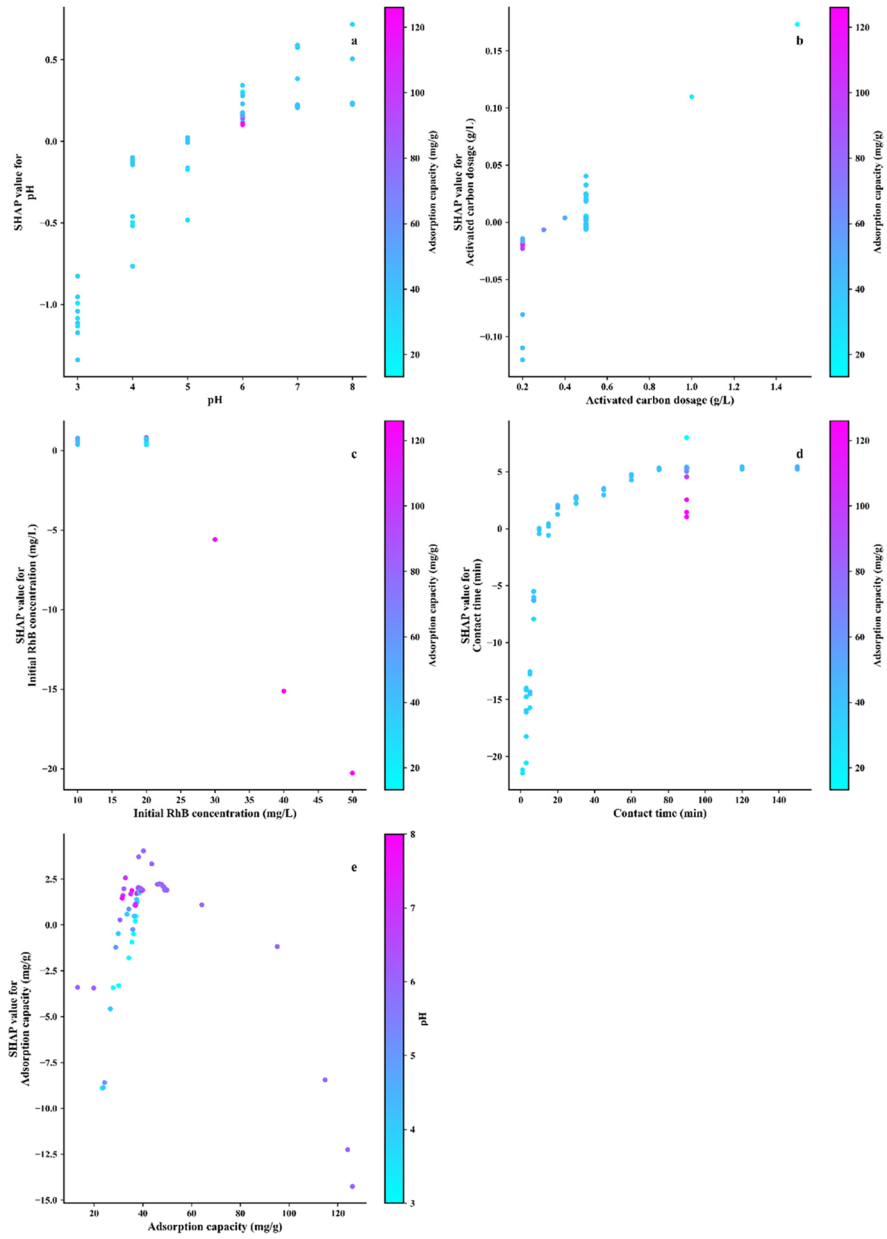

Fig. 18 SHAP dependence plots showing the interaction effects of **a** pH, **b** biochar dose, **c** initial RhB concentration, **d** contact time, and **e** adsorption capacity on RhB removal efficiency. The dependence plots summarize feature effects and interactions, confirming the strong influence of contact time and adsorption capacity on model behaviour

capacity-emphasizing the nonlinear and interdependent nature of operational parameters in dye adsorption systems.

3.4.5 Learning Curve evaluation and Generalization Ability

In order to analyse the generalization ability of the model and its sensitivity to data size, a learning curve evaluation was performed. This analysis reveals the changes in the accuracy performance of the model as the training set size increases.

As illustrated in Fig. 19, the R^2 score of the model on the training set remains consistently high and close to 1.0 for all training sizes, confirming that the model learned the training data effectively. However, for smaller training set sizes, the validation R^2 values are noticeably lower and show substantial fluctuation, indicating limited generalization when insufficient

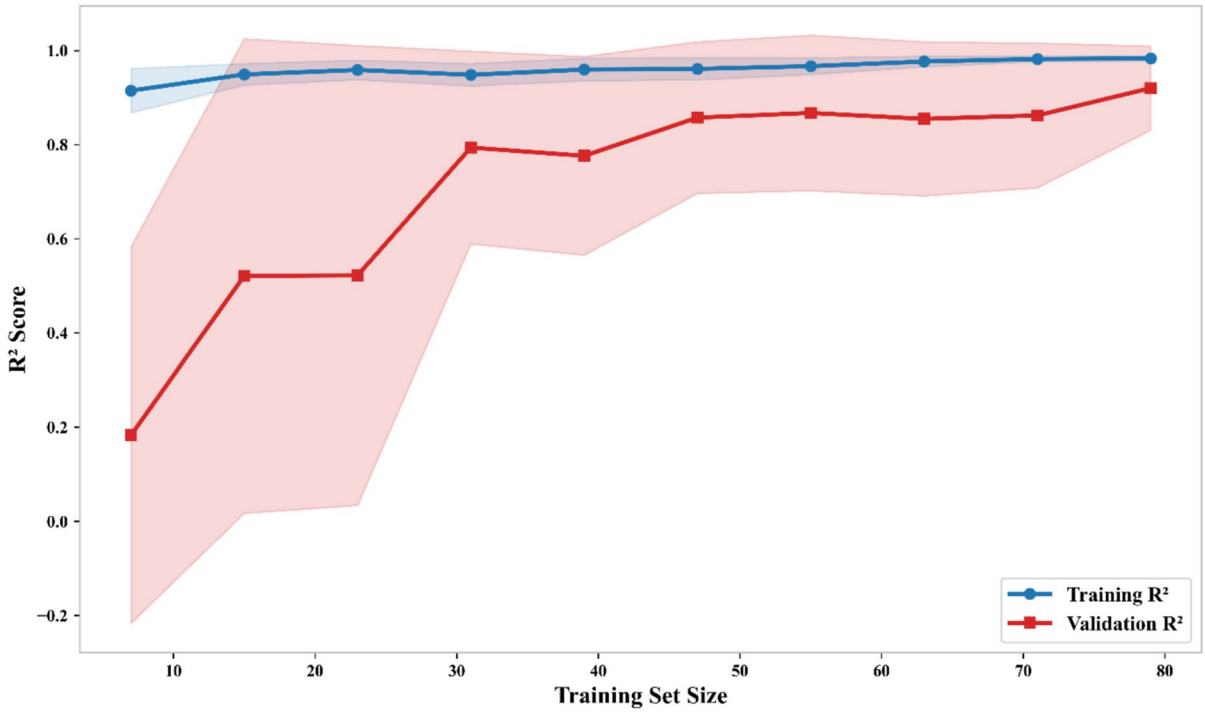

Fig. 19 Learning curve of Random Forest Regressor model

data are available. As the number of training samples increased, the validation R^2 score showed a clear upward trend, and the variance among validation folds became visibly narrower. After approximately 60 samples, the validation curve aligns more closely with the training curve, demonstrating improved model stability and generalization. This pattern shows that the model is more prone to overfitting when trained on small datasets, but this effect diminishes progressively as the training size expands. Overall, the learning curve confirms that enlarging the dataset substantially enhances the model's generalization ability and predictive reliability.

3.4.6 Residual Error Analysis and Model Bias Assessment

Residual analysis was performed to evaluate the model's prediction errors and to determine whether there is systematic bias or deviation. The random and near-zero distribution of the residuals indicates that the model provides balance and stability in its predictions.

As seen in Fig. 20, the residuals in both the training and test sets are largely distributed around zero. This shows that the model generally produces accurate predictions in both the training and validation stages. Most points fall within a narrow residual band, showing that the Random Forest model captures the underlying patterns effectively. However, a small number of test samples (~5%) exhibit large negative residuals, meaning that the model overestimates the removal efficiency for several low-performance cases. Such deviations typically occur in the presence of outliers or data regions with limited representation. Despite these few anomalies, the overall random and structureless distribution of residuals confirms the absence of systematic bias, suggesting that the model does not consistently overpredict or underpredict across the dataset. The residual spread also supports the conclusion that the model preserves strong generalizability without signs of overfitting (Breinholt et al., 2012). As a result, it can be said that the model maintains balance in both the training and test data and does not exhibit overfitting behaviour.

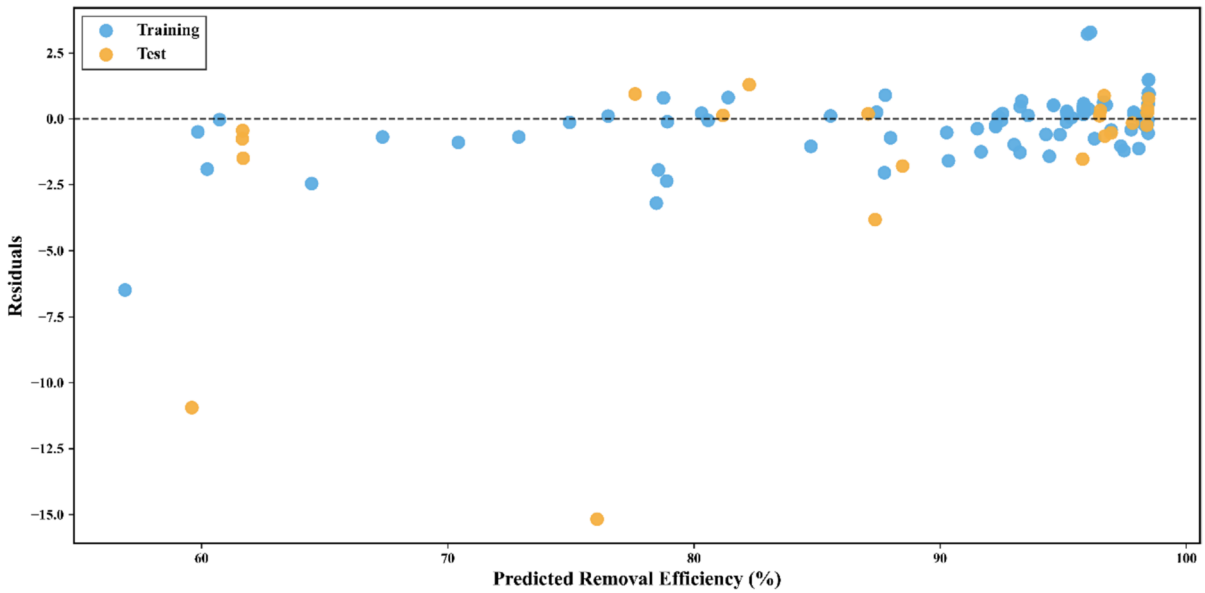

Fig. 20 Residual graph of the Random Forest Regressor model

3.5 Alignment with Current Biochar–ML Studies

Among the models evaluated in this study, the Random Forest algorithm provided the highest predictive accuracy on the test set ($R^2 = 0.93$, RMSE = 4.15, MAE = 1.95), capturing the nonlinear behaviour of the system without signs of overfitting. SHAP analysis revealed that contact time and adsorption capacity exert the strongest influence on the model decisions, a trend that aligns closely with the dominant role of C_0 and operational parameters reported in recent biochar–ML studies. Liu et al. (2025) similarly identified experimental conditions as the primary contributors (50.8%) to CatBoost predictions, while Yadav et al. (2025) and Rajput et al. (2025) also emphasised concentration-to-dosage ratios and BET surface area as key determinants of adsorption performance. In our model, partial dependence plots clarified the marginal effects of individual variables, and the learning curves and residual analyses consistently confirmed the model's stability and generalisation capability. Compared with the near-ideal accuracies achieved in highly curated, single-dye datasets ($R^2 \approx 0.98$–0.99), the slightly lower performance observed here is expected given the broader heterogeneity of experimental conditions incorporated into the present dataset. Importantly, the coherence between our feature importance patterns and those reported in the latest ML–biochar literature demonstrates that the Random Forest model successfully learns the mechanistic signals governing dye removal while maintaining strong predictive performance across diverse operational ranges.

4 Conclusion

In this study, it was aimed to remove Rhodamine B (RhB) dye from aqueous media effectively and sustainably using composite biochar obtained from seaweed species *Ulva lactuca –Cystoseira sl.*. Structural data obtained as a result of SEM, FTIR and BET analyses revealed that the adsorbent has an effective adsorption capacity due to its high surface area (797.91 m^2/g) and porous structure. Kinetic analyses showed that the system is suitable for pseudo-second-order kinetics and chemical interactions are dominant. In isotherm analyses, the Freundlich model successfully reflected the heterogeneous character of the adsorbent surface and the multilayer adsorption mechanism. Modelling studies conducted with machine learning approaches revealed that the Random Forest algorithm can predict RhB removal with high accuracy ($R^2 = 0.93$, RMSE = 4.15, MAE = 1.95). With SHAP analysis, the decision mechanism of the model

has been made transparent, and the decisive effects of contact time and adsorption capacity on the predictions have been emphasized. PDP and learning curve analyses have shown that the model can produce decisions consistent with the physical system and that its generalization ability is strong. As a result, this study reveals that both biomass waste can be converted into environmentally friendly adsorbents and that machine learning-based models can be integrated into water treatment technologies and make significant contributions to the process. This approach constitutes a strong example for sustainable environmental management and data-driven optimization strategies.

Author Contributions All authors contributed to the study conception and design. Material preparation, data collection and analysis were performed by Dilek Gümüş and Fatih Gümüş. The first draft of the manuscript was written by Elif Nihan Kadıoğlu and Handan Atalay Eroğlu and all authors commented on previous versions of the manuscript. All authors read and approved the final manuscript.

Funding The authors did not receive support from any organization for the submitted work.

Data Availability The data will be made available on reasonable request from corresponding author.

Declarations

Ethical Approval This does not apply to this study as no human or animal subjects were involved.

Consent to Participate All authors agreed with the content, and all gave explicit consent to submit, and they obtained consent from the responsible authorities at the institute/organization where the work has been carried out, before the work is submitted.

Consent for Publication This manuscript is approved by all authors for publication in Water, Air, & Soil Pollution.

Competing Interests The authors declare no competing interests.

References

Abekoon, T., Premarathne, W. M. A. C., Jayasekara, J. M. K. P., & Hettiarachchi, H. A. K. (2025). A novel application with explainable machine learning (SHAP and LIME) to predict soil N, P, and K nutrient content in cabbage cultivation. *Smart Agricultural Technology, 11*, Article 100879. https://doi.org/10.1016/j.atech.2025.100879

Ahmad, M. A., & Alrozi, R. (2011). Removal of malachite green dye from aqueous solution using rambutan peel-based activated carbon: Equilibrium, kinetic and thermodynamic studies. *Chemical Engineering Journal, 171*(2), 510–516. https://doi.org/10.1016/j.cej.2011.04.018

Ahmad, M. A., & Rahman, N. K. (2011). Equilibrium, kinetics and thermodynamic of Remazol Brilliant Orange 3R dye adsorption on coffee husk-based activated carbon. *Chemical Engineering Journal, 170*(1), 154–161. https://doi.org/10.1016/j.cej.2011.03.045

Ahmad, M., Lee, S. S., Dou, X., Mohan, D., Sung, J. K., Yang, J. E., & Ok, Y. S. (2014). Biochar as a sorbent for contaminant management in soil and water: A review. *Chemosphere, 99*, 19–33. https://doi.org/10.1016/j.chemosphere.2013.10.071

Alraae, A., Alfadhel, A., Alsaedi, A., Alqadami, A. A., & Naushad, M. (2025). Assessing the effects of reaction variables for enhanced chromium(III) adsorption efficiency using beidellite clay. *Results in Surfaces and Interfaces, 19*, Article 100523. https://doi.org/10.1016/j.rsurfi.2025.100523

Arabzadeh Nosratabad, N., Akbari, A., & Shokri, B. (2024). Exploring nanomaterial-modified biochar for environmental remediation applications. *Heliyon, 10*(18), Article e37123. https://doi.org/10.1016/j.heliyon.2024.e37123

Ashraf, M., Rehman, R., Hatshan, M. R., Bathula, C., Dar, A., & Akram, M. (2024). Process modeling of methylene blue dye adsorptive removal by physio-chemically treated *Cicer arietinum* husk for effective wastewater treatment by green chemistry. *Water, Air, and Soil Pollution, 235*(5), 267. https://doi.org/10.1007/s11270-024-07052-1

Atalay Eroğlu, H., Kadıoğlu, E. N., & Akbal, F. (2025). High-efficiency removal of Rhodamine B using modified biochar from agricultural waste pine nut shell: Investigation of kinetics, isotherms, and artificial neural network modeling. *Biomass Conversion and Biorefinery, 15*(8), 12137–12150. https://doi.org/10.1007/s13399-024-06045-8

Baskar, A. V., Deepthi, A. S., Sivalingam, V., Gopalakrishnan, D., Arumugam, M., Venkatachalam, S., & Rajendran, S. (2022). Recovery, regeneration and sustainable management of spent adsorbents from wastewater treatment streams: A review. *Science of the Total Environment, 822*, Article 153555. https://doi.org/10.1016/j.scitotenv.2022.153555

Behera, A. K., Shadangi, K. P., & Sarangi, P. K. (2024). Efficient removal of Rhodamine B dye using biochar as an adsorbent: Study the performance, kinetics, thermodynamics, adsorption isotherms and its reusability. *Chemosphere, 354*, Article 141702. https://doi.org/10.1016/j.chemosphere.2024.141702

Bhatnagar, A., & Sillanpää, M. (2010). Utilization of agro-industrial and municipal waste materials as potential adsorbents for water treatment—A review. *Chemical Engineering Journal, 157*(2), 277–296. https://doi.org/10.1016/j.cej.2010.01.007

Breinholt, A., Madsen, H., Thordarson, F. O., Rosbjerg, D., & Jensen, K. H. (2012). A formal statistical approach to representing uncertainty in rainfall–runoff modelling

with focus on residual analysis and probabilistic output evaluation – Distinguishing simulation and prediction. *Journal of Hydrology, 472–473*, 36–52. https://doi.org/10.1016/j.jhydrol.2012.09.014

Crini, G. (2006). Non-conventional low-cost adsorbents for dye removal: A review. *Bioresource Technology, 97*(9), 1061–1085. https://doi.org/10.1016/j.biortech.2005.05.001

Crini, G., & Badot, P.-M. (2008). Application of chitosan, a natural aminopolysaccharide, for dye removal from aqueous solutions by adsorption processes using batch studies: A review of recent literature. *Progress in Polymer Science, 33*(4), 399–447. https://doi.org/10.1016/j.progpolymsci.2007.11.001

Crini, G., & Lichtfouse, E. (2019). Advantages and disadvantages of techniques used for wastewater treatment. *Environmental Chemistry Letters, 17*(1), 145–155. https://doi.org/10.1007/s10311-018-0785-9

Esu, C. O., Pyo, J., & Cho, K. (2024). Machine learning-derived dose-response relationships considering interactions in mixtures: Applications to the oxidative potential of particulate matter. *Journal of Hazardous Materials, 475*, Article 134864. https://doi.org/10.1016/j.jhazmat.2024.134864

Foo, K. Y., & Hameed, B. H. (2010). Insights into the modeling of adsorption isotherm systems. *Chemical Engineering Journal, 156*(1), 2–10. https://doi.org/10.1016/j.cej.2009.09.013

Foo, K. Y., & Hameed, B. H. (2012). A cost effective method for regeneration of durian shell and jackfruit peel activated carbons by microwave irradiation. *Chemical Engineering Journal, 193*, 404–409. https://doi.org/10.1016/j.cej.2012.04.055

Foong, S. Y., Liew, R. K., Yang, Y., Peng, W., Lee, X. J., & Gan, S. (2023). Recent progress in the production and application of biochar and its composite in environmental biodegradation. *Bioresource Technology, 387*, Article 129592. https://doi.org/10.1016/j.biortech.2023.129592

Fu, J., Chen, Z., Wang, M., Liu, S., Zhang, J., Zhang, J., & Xu, Q. (2015). Adsorption of methylene blue by a high-efficiency adsorbent (polydopamine microspheres): Kinetics, isotherm, thermodynamics and mechanism analysis. *Chemical Engineering Journal, 259*, 53–61. https://doi.org/10.1016/j.cej.2014.07.101

Ghafarian, F., Seifollahi-Aghmiuni, S., Hassani, H., & Golian, S. (2022). Application of extreme gradient boosting and Shapley additive explanations to predict temperature regimes inside forests from standard open-field meteorological data. *Environmental Modelling & Software, 156*, Article 105466. https://doi.org/10.1016/j.envsoft.2022.105466

Gümüş, D., & Gümüş, F. (2022). Removal of hydroxychloroquine using engineered biochar from algal biodiesel industry waste: Characterization and design of experiment (DoE). *Arabian Journal for Science and Engineering, 47*(6), 7325–7334. https://doi.org/10.1007/s13369-021-06235-w

Gupta, V. K., & Nayak, A. (2012). Cadmium removal and recovery from aqueous solutions by novel adsorbents prepared from orange peel and Fe2O3 nanoparticles. *Chemical Engineering Journal, 180*, 81–90. https://doi.org/10.1016/j.cej.2011.11.006

Gupta, V. K., & Suhas. (2009). Application of low-cost adsorbents for dye removal – A review. *Journal of Environmental Management, 90*(8), 2313–2342. https://doi.org/10.1016/j.jenvman.2008.11.017

Hameed, B. H., Din, A. T. M., & Ahmad, A. L. (2007). Adsorption of methylene blue onto bamboo-based activated carbon: Kinetics and equilibrium studies. *Journal of Hazardous Materials, 141*(3), 819–825. https://doi.org/10.1016/j.jhazmat.2006.07.049

Hashem, A., Khaleel, M., Ibrahim, W. M., El-Eswed, B., & Mahmoud, M. E. (2024). Evaluation of the adsorption capacity of surfactant-modified biomass in an aqueous acid blue 193 system. *Waste Management Bulletin, 2*(1), 172–183. https://doi.org/10.1016/j.wmb.2024.01.004

Hernández-Abreu, A. B., González, R. S., & Sánchez-Silva, L. (2020). New insights from modelling and estimation of mass transfer parameters in fixed-bed adsorption of Bisphenol A onto carbon materials. *Journal of Contaminant Hydrology, 228*, Article 103566. https://doi.org/10.1016/j.jconhyd.2019.103566

Ho, Y. S., & McKay, G. (1999). Pseudo-second order model for sorption processes. *Process Biochemistry, 34*(5), 451–465. https://doi.org/10.1016/S0032-9592(98)00112-5

Hoang, L. T. T. T., Pham, T. A., Tran, M. T. T., Doan, V. D., & Le, T. T. (2024). Utilization of dragon fruit (*Hylocereus undatus*) peel-derived biochar for the adsorptive removal of tetracycline from aqueous solution. *International Journal of Phytoremediation, 26*(14), 2313–2324. https://doi.org/10.1080/15226514.2024.2389471

Hou, Y., Huang, G., Li, J., Yang, Q., Huang, S., & Cai, J. (2019). Hydrothermal conversion of bamboo shoot shell to biochar: Preliminary studies of adsorption equilibrium and kinetics for rhodamine B removal. *Journal of Analytical and Applied Pyrolysis, 143*, Article 104694. https://doi.org/10.1016/j.jaap.2019.104694

Hu, Q., Liu, Y., Feng, C., Zhang, Z., Lei, Z., & Shimizu, K. (2018). Predicting equilibrium time by adsorption kinetic equations and modifying Langmuir isotherm by fractal-like approach. *Journal of Molecular Liquids, 268*, 728–733. https://doi.org/10.1016/j.molliq.2018.07.113

Inyang, M. I., Gao, B., Yao, Y., Xue, Y., Zimmerman, A. R., Mosa, A., Pullammanappallil, P., Ok, Y. S., & Cao, X. (2016). A review of biochar as a low-cost adsorbent for aqueous heavy metal removal. *Critical Reviews in Environmental Science and Technology, 46*(4), 406–433. https://doi.org/10.1080/10643389.2015.1096880

Jawad, A. H., Abdulhameed, A. S., Bahrudin, N. N., Hum, N. N. M. F., Surip, S. N., Syed-Hassan, S. S. A., & Sabar, S. (2021). Microporous activated carbon developed from KOH activated biomass waste: Surface mechanistic study of methylene blue dye adsorption. *Water Science and Technology, 84*(8), 1858–1872. https://doi.org/10.2166/wst.2021.355

Kapoor, R. T., Rafatullah, M., Siddiqui, M. R., & Alam, M. (2024). Adsorptive potential of coconut fruit shell biochar as low-cost adsorbent for sequestration of rhodamine B dye: Kinetics, thermodynamics and phytotoxicity studies. *Biomass Conversion and Biorefinery*. https://doi.org/10.1007/s13399-024-05688-x

Kayranli, B. (2025). Adsorption efficiency of groundnut husk biochar in reduction of rhodamine B, recycle, and reutilization. *Biomass Conversion and Biorefinery*. https://doi.org/10.1007/s13399-025-06781-5

Kumar, A., Singh, E., & Lo, S.-L. (2025). Tunable 2D porous Ti3C2Tx MXene@biochar composites synthesized via ultrasound-assisted self-assembly for simultaneous removal of co-existing wastewater contaminants. *Separation and Purification Technology, 355*, Article 129648. https://doi.org/10.1016/j.seppur.2024.129648

Li, N., Thomas, R. K., & Rennie, A. R. (2012). Effect of pH, surface charge and counter-ions on the adsorption of sodium dodecyl sulfate to the sapphire/solution interface. *Journal of Colloid and Interface Science, 378*(1), 152–158. https://doi.org/10.1016/j.jcis.2012.04.026

Li, P., Zhao, T., Zhao, Z., Tang, H., Feng, W., & Zhang, Z. (2023). Biochar derived from Chinese herb medicine residues for rhodamine B dye adsorption. *ACS Omega, 8*(5), 4813–4825. https://doi.org/10.1021/acsomega.2c06968

Li, C., Chen, S., Zhang, Y., Wang, J., & Liu, J. (2025a). Machine learning-driven prediction of nitrate-N adsorption efficiency by Fe-modified biochar: Refined model tuning and identification of crucial features. *Journal of Water Process Engineering, 70*, Article 107026. https://doi.org/10.1016/j.jwpe.2025.107026

Li, W., Xu, Y., Guo, X., Chen, G., Wang, H., & Li, M. (2025b). Machine learning-based prediction and model interpretability analysis for algal growth affected by microplastics. *Science of the Total Environment, 958*, Article 178003. https://doi.org/10.1016/j.scitotenv.2024.178003

Lin, L., Zhang, S., Wang, P., Wang, H., Zhang, C., Liu, J., & Zhang, W. (2020). Accumulation mechanism of tetracycline hydrochloride from aqueous solutions by nylon microplastics. *Environmental Technology & Innovation, 18*, Article 100750. https://doi.org/10.1016/j.eti.2020.100750

Liu, Y. (2008). New insights into pseudo-second-order kinetic equation for adsorption. *Colloids and Surfaces A: Physicochemical and Engineering Aspects, 320*(1), 275–278. https://doi.org/10.1016/j.colsurfa.2008.01.032

Liu, C., Balasubramanian, P., Nguyen, X. C., An, J., Praneeth, S., Zhang, P., & Huang, H. (2025). Enhanced machine learning prediction of biochar adsorption for dyes: Parameter optimization and experimental validation. *Carbon Research, 4*(1), 46. https://doi.org/10.1007/s44246-025-00213-9

Lundberg, S. M., Erion, G., Chen, H., DeGrave, A., Prutkin, J. M., Nair, B., Katz, R., Himmelfarb, J., Bansal, N., & Lee, S.-I. (2020). From local explanations to global understanding with explainable AI for trees. *Nature Machine Intelligence, 2*(1), 56–67. https://doi.org/10.1038/s42256-019-0138-9

Ma, R., Nie, D., Sang, M., Wang, W., & Nie, G. (2023). Adsorption of rhodamine B and Pb (II) from aqueous solution by MoS2 nanosheet modified biochar: Fabrication, performance, and mechanisms. *Bioresource Technology, 386*, Article 129548. https://doi.org/10.1016/j.biortech.2023.129548

Mayilswamy, N., Kandasubramanian, B., & Gore, A. (2025). ANN-based predictive modelling for optimizing Rhodamine B removal from aqueous matrices using ball-milled sewage sludge biochar. *Materials Today Communications*. https://doi.org/10.1016/j.mtcomm.2025.112798

Mohan, D., Sarswat, A., Ok, Y. S., & Pittman, C. U., Jr. (2014). Organic and inorganic contaminants removal from water with biochar, a renewable, low cost and sustainable adsorbent – A critical review. *Bioresource Technology, 160*, 191–202. https://doi.org/10.1016/j.biortech.2014.01.120

Mousavi, S. A., Kamarehie, B., Almasi, A., Darvishmotevalli, M., Salari, M., Moradnia, M., & Karami, M. A. (2023). Removal of Rhodamine B from aqueous solution by stalk corn activated carbon: Adsorption and kinetic study. *Biomass Conversion and Biorefinery, 13*(9), 7927–7936. https://doi.org/10.1007/s13399-021-01628-1

Niedzbała, N., Pietrzak, M., Michalska-Pożoga, I., Stachowiak, T., & Kaniuczak, J. (2024). Potential use of *Ulva intestinalis*-derived biochar adsorbing phosphate ions in the cultivation of winter wheat *Tristicum aestivum*. *Bioresources and Bioprocessing, 11*(1), 27. https://doi.org/10.1186/s40643-024-00741-z

Oliveira, M. G., Freitas, J. G., Reis, C., Pinto, A. M. F. R., & Loureiro, J. M. (2023). Adsorption kinetics of ciprofloxacin and ofloxacin by green-modified carbon nanotubes. *Environmental Research, 233*, Article 116503. https://doi.org/10.1016/j.envres.2023.116503

Ozcan, D. O., Hendekci, M. C., & Ovez, B. (2024). Enhancing the adsorption capacity of organic and inorganic pollutants onto impregnated olive stone derived activated carbon. *Heliyon, 10*(12), Article e32792. https://doi.org/10.1016/j.heliyon.2024.e32792

Pompeu, L. D., Umpiérrez, F. S., da Silva, E. A., & Pinto, L. A. A. (2023). Adsorption of Rhodamine B dye onto novel biochar: Isotherm, kinetic, thermodynamic study and antibiofilm activity. *Inorganic Chemistry Communications, 158*, Article 111509. https://doi.org/10.1016/j.inoche.2023.111509

Rafatullah, M., Sulaiman, O., Hashim, R., & Ahmad, A. (2010). Adsorption of methylene blue on low-cost adsorbents: A review. *Journal of Hazardous Materials, 177*(1), 70–80. https://doi.org/10.1016/j.jhazmat.2009.12.047

Rajput, P., Yadav, S., Liu, C., & Balasubramanian, P. (2025). Predicting biochar adsorption capacity for methylene blue removal using machine learning. *Journal of Water Process Engineering, 69*, Article 106749. https://doi.org/10.1016/j.jwpe.2024.106749

Ravindiran, G., Muthunarayanan, M., Murugesan, T., & Maruthamuthu, V. (2024). Conversion of seaweed waste to biochar for the removal of heavy metal ions from aqueous solution: A sustainable method to address eutrophication problem in water bodies. *Environmental Research, 241*, Article 117551. https://doi.org/10.1016/j.envres.2023.117551

Salleh, M. A. M., Mahmoud, D. K., Karim, W. A. W. A., & Idris, A. (2011). Cationic and anionic dye adsorption by agricultural solid wastes: A comprehensive review. *Desalination, 280*(1), 1–13. https://doi.org/10.1016/j.desal.2011.07.019

Satayev, M., Zdorovets, M., Kozlovskiy, A., Shlimas, D., Sarsenbekuly, B., Karimova, M., & Kaikenov, M. (2024). Modeling of the adsorption allowing for the changing adsorbent activity at various stages of the process.

Frontiers in Heat and Mass Transfer, 22(5), 1533–1558. https://doi.org/10.32604/fhmt.2024.052901

Siddique, A. B., Al-Dhafeeri, A. M., Afaq, S., Naushad, M., Alothman, Z. A., & Alam, M. M. (2025). Tree-based, boosting, and stacked models for accurate prediction of total organic carbon from conventional well logs. *Energy Reports, 13*, 4491–4513. https://doi.org/10.1016/j.egyr.2025.04.021

Soares Dias, A. P., Costa, L. M., Miranda, M. S., Amorim, E. P., & Nascimento, E. S. (2025). Seaweed-derived biochar for effective treatment of dye-contaminated wastewater. *Water, 17*(8), 1215. https://doi.org/10.3390/w17081215

Su, Y., Zheng, Y., Feng, M., & Chen, S. (2022). Magnetic luffa-leaf-derived hierarchical porous biochar for efficient removal of rhodamine B and tetracycline hydrochloride. *International Journal of Molecular Sciences, 23*(24), 15703. https://doi.org/10.3390/ijms232415703

Tan, X., Liu, Y., Zeng, G., Wang, X., Hu, X., Gu, Y., & Yang, Z. (2015). Application of biochar for the removal of pollutants from aqueous solutions. *Chemosphere, 125*, 70–85. https://doi.org/10.1016/j.chemosphere.2014.12.058

Tang, W.-W., Zeng, G.-M., Gong, J.-L., Liu, Y., Wang, X., Liu, Y.-Y., & Liu, Z.-F. (2014). Impact of humic/fulvic acid on the removal of heavy metals from aqueous solutions using nanomaterials: A review. *Science of the Total Environment, 468–469*, 1014–1027. https://doi.org/10.1016/j.scitotenv.2013.09.044

Tedoldi, D., Moretti, M., Re, V., & Hynds, P. D. (2025). Common mistakes and solutions for a better use of correlation- and regression-based approaches in environmental sciences. *Environmental Modelling & Software, in Press.* https://doi.org/10.1016/j.envsoft.2025.106526

Tomasella, P., Goetzke, V., Gauglitz, P.-A., Maier, M., Vossmeyer, T., & Lisdat, F. (2025). Time-resolved study of nanoparticle adsorption at liquid surfaces: Structure, thermodynamics and kinetics. *Journal of Colloid and Interface Science, in Press.* https://doi.org/10.1016/j.jcis.2025.137978

Ullah, H., Yang, Y., Tang, L., Liu, Z., Geng, Y., & Wang, J. (2023). Machine learning approach to predict adsorption capacity of Fe-modified biochar for selenium. *Carbon Research, 2*(1), 29. https://doi.org/10.1007/s44246-023-00061-5

Wang, J., Zhang, X., Li, Y., Zhang, M., Wang, H., & Zhang, W. (2023). On the adsorption characteristics and mechanism of methylene blue by ball mill modified biochar. *Scientific Reports, 13*(1), 21174. https://doi.org/10.1038/s41598-023-48373-1

Wu, J., Yang, J., Huang, G., Xu, C., & Lin, B. (2020). Hydrothermal carbonization synthesis of cassava slag biochar with excellent adsorption performance for Rhodamine B. *Journal of Cleaner Production, 251*, Article 119717. https://doi.org/10.1016/j.jclepro.2019.119717

Xie, G., Zhang, Y., Wang, J., Zhao, X., & Zhang, W. (2025). Predicting the adsorption of ammonia nitrogen by biochar in water bodies using machine learning strategies: Model optimization and analysis of key characteristic variables. *Environmental Research, 267*, Article 120618. https://doi.org/10.1016/j.envres.2024.120618

Yadav, S., Singh, A., Kumar, A., Mishra, A., Singh, R., Kumar, S., & Raghubanshi, A. S. (2025). Machine learning-driven prediction of biochar adsorption capacity for effective removal of Congo red dye. *Carbon Research, 4*(1), 11. https://doi.org/10.1007/s44246-024-00168-3

Yang, J., Wei, Q., Li, D., Yu, J., & Cai, Z. (2023). Study on adsorption performance of manganese titanium oxide composite biochar for removal of Rhodamine B. *Journal of the Indian Chemical Society, 100*(4), Article 100958. https://doi.org/10.1016/j.jics.2023.100958

Zhang, W., Wu, L., Xue, Y., Li, Y., Li, J., & Xu, Z. (2023). Synthesis optimization and adsorption modeling of biochar for pollutant removal via machine learning. *Biochar, 5*(1), 25. https://doi.org/10.1007/s42773-023-00225-x

Zhang, D., Li, Z., Wang, C., Li, M., & Wang, H. (2025). Multimechanism synergistic adsorption of lead and cadmium in water by structure-functionally adapted modified biochar: A review. *Desalination and Water Treatment, 322*, Article 101156. https://doi.org/10.1016/j.dwt.2025.101156

Zhao, Y., Wang, X., Li, C., Zhou, J., Zhang, X., & Xu, L. (2022). Application of machine learning in predicting the adsorption capacity of organic compounds onto biochar and resin. *Environmental Research, 208*, Article 112694. https://doi.org/10.1016/j.envres.2022.112694

Zhao, C., Zhang, W., Gao, B., Peng, B., & Peng, X. (2024). Reveal the main factors and adsorption behavior influencing the adsorption of pollutants on natural mineral adsorbents: Based on machine learning modeling and DFT calculation. *Separation and Purification Technology, 331*, Article 125706. https://doi.org/10.1016/j.seppur.2023.125706

Publisher's Note Springer Nature remains neutral with regard to jurisdictional claims in published maps and institutional affiliations.

Springer Nature or its licensor (e.g. a society or other partner) holds exclusive rights to this article under a publishing agreement with the author(s) or other rightsholder(s); author self-archiving of the accepted manuscript version of this article is solely governed by the terms of such publishing agreement and applicable law.